PREPARATION AND APPLICATION OF SUBNANO CERAMIC FILTRATION MEMBRANES FOR ORGANIC SPECIES REMOVAL FROM AQUEOUS STREAMS

A Thesis Submitted to
the Graduate School of Engineering and Sciences of
İzmir Institute of Technology
in Partial Fulfillment of the Requirements for the Degree of

MASTER OF SCIENCE

in Chemical Engineering

by
Kaan YALTRIK

July 2017
İZMİR

We approve the thesis of **Kaan YALTRIK**

Examining Committee Members:

Prof. Dr. Muhsin ÇİFTÇİOĞLU
Department of Chemical Engineering, İzmir Institute of Technology

Assist. Prof. Dr. Umut ADEM
Department of Materials Science and Engineering, İzmir Institute of Technology

Assoc. Prof. Dr. Emre YALAMAÇ
Department of Metallurgy and Materials Engineering, Manisa Celal Bayar University

24 July 2017

Prof. Dr. Muhsin ÇİFTÇİOĞLU
Supervisor, Department of Chemical Engineering
İzmir Institute of Technology

Prof. Dr. Fehime ÇAKICIOĞLU ÖZKAN
Head of the Department of Chemical Engineering

Prof. Dr. Aysun SOFUOĞLU
Dean of the Graduate School of Engineering and Sciences

ACKNOWLEDGEMENTS

It is a genuine pleasure to express my immeasurable appreciation and deepest gratitude to Dr. Muhsin ÇİFTÇİOĞLU for his precious guidance and support, understanding and encouragements throughout my graduate education and in the preparation of this thesis and also for the productive environment that he built in his laboratories.

My appreciation extends to my colleagues; Pınar ÇETİN, Öncel KIRKBAŞ, İklima ODABAŞI, Safiye YALDIZ, Kenan YILMAZ (Alphabetical Order) for their support and encouragement during the laboratory work. Moreover, I am greatly indebted to Dr. Burcu ALP, Dr. Ali Emrah ÇETİN, Rukiye ÇİFTÇİOĞLU and Dr. Hüsnü Arda YURTSEVER for their guidance, endless support and foremost their precious friendship.

Thank you to my girlfriend Deniz ANGI, for all her love, understanding and support.

Above all, I am most grateful to my dear parents for their eternal support, never ending love and encouragement during all my educational life.

I would like to thank İzmir Institute of Technology Center For Materials Research (IZTECH MAM) for providing technical support and help. I would also like to thank Middle East Technical University (METU) Central Laboratory for TEM characterizations.

The studies in this thesis was funded by the Scientific and Technological Research Council of Turkey (TUBITAK) within the context of Çevre, Atmosfer, Yer ve Deniz Bilimleri Araştırma Destek Grubu (ÇAYDAG) 113Y344 project.

ABSTRACT

PREPARATION AND APPLICATION OF SUBNANO CERAMIC FILTRATION MEMBRANES FOR ORGANIC SPECIES REMOVAL FROM AQUEOUS STREAMS

The purpose of this MSc work was to investigate the effects of neodymium/zirconium doping on the phase structure evolution of the selective titania nanofiltration (NF) membrane layers for the rejection of subnano sized organic compounds. A dilatometric study was carried out on unsupported membranes prepared from polymeric sols with different neodymium and zirconium levels. The development of functional abilities towards the design of the pore structure in the subnano range by controlling the nanostructural evolution of the selective NF layers was the fundamental purpose of this work. The neodymium doping level was varied in the 0.3-5.0% range and the zirconium mixing level was varied in the 0-100% range based on stable metal oxide molar compositions.

Dilatometric characterization results have shown that dopant level effects the nanophase evolution and the densification behavior considerably. The dynamic light scattering results have shown that the polymeric species in the sol were predominantly 2-4 nm in size and had a very narrow size distribution. XRD analysis results indicated titania anatase crystallite sizes were reduced significantly with neodymium doping or zirconia mixing and the phase transformations were retarded by about 200°C. HR-TEM images of selected zirconia mixed or neodymium doped unsupported membrane powders also added new information to the XRD/dilatometry derived nanophase evolution results. The determination of the molecular weight cut-off values and pure water fluxes of the NF membranes which would be prepared by using these polymeric sols in the near future may generate valuable knowledge on the subnano separation abilities of these NF membranes.

ÖZET

SU BAZLI KARIŞIMLARDAN ORGANİK YAPILARIN AYRIMINA YÖNELİK NANOALTI SERAMİK FİLTRASYON MEMBRANLARININ HAZIRLANMASI VE UYGULANMASI

Bu yüksek lisans çalışmasının amacı nanoaltı boyuttaki organik bileşiklerin tutulmasında kullanılması amaçlanan seçici titanya nanofiltrayson (NF) membran katmanlarının faz yapısı evrimine neodmiyum/zirkonyum katkılarının etkilerinin araştırılmasıdır. Farklı neodmiyum ve zirkonyum katkı düzeylerindeki polimerik sollerden hazırlanan desteksiz membranlar ile dilatometrik bir çalışma yürütülmüştür. Seçici NF katmanlarının nanoyapı evriminin kontrolü ile birlikte nanoaltı gözenek yapısı tasarımı üzerine fonksiyonel becerilerin geliştirilmesi bu çalışmanın temel amacını oluşturmuştur. Kararlı oksit molar bileşimleri baz alınarak neodmiyum katkı düzeyi 0.3-5.0% aralığında, zirkonyum karışım düzeyi ise 0-100% aralığında değiştirilmiştir.

Dilatometrik karakterizasyon sonuçları katkı düzeylerinin nanoyapı evrimini ve yoğunlaşma davranışlarını önemli oranda etkilediğini göstermektedir. Dinamik ışık saçılımı sonuçları sollerdeki polimerik yapıların ağırlıklı olarak 2-4 nm boyutunda olduğunu ve oldukça dar bir boyut dağılımına sahip olduğunu göstermektedir. XRD analizi sonuçları titanya anataz kristalit boyutlarının neodmiyum katkısı veya zirkonya karışımı ile önemli ölçüde düştüğünü ve faz dönüşümlerinin yaklaşık olarak 200°C geciktiğini göstermiştir. Seçilmiş zirkonya karışık ve neodmiyum katkılı katkısız membran tozlarının HR-TEM görüntüleri XRD/dilatometre kaynaklı nanoyapı evrimi sonuçlarına yeni bilgiler eklemiştir. Bu polimerik soller kullanılarak hazırlanacak NF membranlarının molekül ağırlığı ayırma sınırlarının ve saf su akılarının yakın gelecekte belirlenmesi nanoaltı ayırma becerileri üzerine değerli bir bilgi birikimi oluşturmasını mümkün kılabilir.

TABLE OF CONTENTS

LIST OF FIGURES

Figure **Page**

LIST OF TABLES

Table **Page**

CHAPTER 1

INTRODUCTION

A membrane is a selective barrier between two phases that prevents intimate contact. Inorganic membranes are first developed and mass produced in the 1940s for uranium enrichment purposes (Gillot 1991). Porous inorganic membranes have two different structures: symmetric membranes and asymmetric membranes. Asymmetric membranes are widely used in the production of ceramic membranes due to their high fluxes.

Nanofiltration (NF) is a pressure-driven membrane process between ultrafiltration (UF) and reverse osmosis (RO) in terms of separation size ranges. It has been widely used in various fields including food & beverage, pharmaceutical, water purification (Cai et al. 2015), and radioactive effluent disposal applications (Lu et al. 2016). The NF process is known to reject small molecules and multivalent ions in the range of 200-1000 Da (Lu et al. 2016) and have the potential to remove organic species from aqueous media (Tsuru et al. 2008, Zeidler et al. 2014, Chen et al. 2017).

The NF membranes can be classified into two groups on a materials basis as organic polymeric and inorganic membranes (Van Gestel et al. 2002). Ceramic NF membranes are attracting significant application/research interest due to their superior chemical, thermal and mechanical stability compared to their organic polymeric counterparts. NF ceramic membranes have been prepared by using various oxides such as titania (TiO_2) (Benfer et al. 2001, Van Gestel et al. 2002, Van Gestel et al. 2003, Voigt et al. 2003, Tsuru et al. 2008), zirconia (ZrO_2) (Benfer et al. 2001, Van Gestel et al. 2006, Zhu et al. 2015), silica (SiO_2) (Farsi et al. 2017), and γ-alumina (γ-Al_2O_3) (Van Gestel et al. 2002, Van Gestel et al. 2003, Kuzniatsova et al. 2008, Topuz and Çiftçioğlu 2010) in the last 10-15 years.

Nanoporous TiO_2-ZrO_2 mixed-oxide membranes have also been produced by some researchers in order to achieve smaller pore sizes due to their mutual retardation during crystallization and nucleation processes (Aust et al. 2006, Zeidler et al. 2014). SiO_2-ZrO_2 membranes have also been utilized in high-temperature nanofiltration studies because of the higher ability of pore size control of silica and high hydrothermal stability

of zirconia (Puthai et al. 2016). SiO_2-TiO_2 mixed-oxide system was used by Farsi et al. (2017) towards the preparation of similar pore size controlled microporous NF membranes. There are two main routes in sol-gel processes: polymeric sol-gel route and colloidal sol-gel route. Polymeric sol-gel route is capable of forming microporous structures whereas colloidal sol-gel route usually generates mesoporous materials (Aust et al. 2006).

Membrane stability and pore sizes are strongly affected by the nanostructure evolution and the closely related nucleation/crystal growth/phase transformation phenomena in the critical heat treatment stage of the ceramic membrane production process (Lin et al. 1994). Dopants like neodymium and zirconium can be used in order to retard the above events, pore growth and densification through blocking the diffusion path along the titania grain contacts. Sekulić et al. (2004) reported that ZrO_2 doping resulted in retardation of pore growth in TiO_2 and the pore size decreased from 4.5 nm down to 3.6 nm for 20 mol% of ZrO_2. This was attributed to the hindered densification of the structure due to the presence of small ZrO_2 clusters located between the TiO_2 crystallites.

The main objective of this MSc study was to investigate the possibility of improving the performance of tubular membranes by minimizing the defects of the selective NF membrane layers. The effect of neodymium/zirconium doping at low levels on the nanostructural evolution and pore structure of titania membranes were investigated for achieving this goal. The development of a better understanding of the phase transformations, crystallite growth and other structural events occurring in supported/unsupported membranes through a dilatometric study was the fundamental objective. The use of dilatometry combined with X-ray diffraction (XRD) and high-resolution transmission electron microscope (HR-TEM) in order to gain a better understanding of nanostructure evolution in undoped/doped titania membranes was studied within the context of this MSc study.

This thesis is comprised from a series of chapters including a review on inorganic membranes in Chapter 2 followed by Chapter 3 on sol-gel based ceramic membranes. Ceramic nanofiltration top layers are reviewed and discussed in Chapter 4. The materials and techniques utilized are given in Chapter 5 in the experimental chapter followed by the results and discussion given in Chapter 6. This manuscript ends with the main conclusions given in Chapter 7.

CHAPTER 2

INORGANIC MEMBRANES

Ceramic membranes have numerous advantages like high thermal/mechanical /chemical stability, long lifetime, cleanability, high throughput volume, diminished fouling and the ability to control/design pore size/structure. However, the brittle character of ceramic membranes necessitates the need for special configurations and high support quality. Relatively high installation and modification costs and high temperature requirements during sintering process are their major drawbacks. The most widely used selective ceramic membrane materials are titania, zirconia, silica, and alumina.

2.1. History of Inorganic Membranes

The development of inorganic membranes started in the 1940s for uranium enrichment, separation of ^{238}U isotope from fissile ^{235}U isotope, in order to have concentrated ^{235}U to be used either in nuclear weapons or power generating plants. Since the separation by mass spectroscopy was expensive, nuclear industries of some countries (e.g. U.S.A. and France) tried to develop economically feasible industrial processes. Separation of uranium isotopes was performed by using volatile and gaseous compounds such as uranium hexafluoride (UF_6). Gigantic uranium enrichment plants using gaseous diffusion by Knudsen diffusion mechanism was thus established soon afterward. The Commissariat a l' Energie Atomique (CEA), conducted research on inorganic membranes in the 1950s. Tubular macroporous supports of CEA were produced by French companies named Desmarquest, Le Carbone Lorraine, and Copagnie Generale d' Electroceramique (CGEC). At the same time, Societe de Fabrication d' Elements Catalytiques (SFEC) was set up to produce separation layers on supports and to assemble membranes into modules (Gillot 1991). Several European countries including France, Belgium, Spain and Italy established the Eurodif gas diffusion plant after the outbreak of oil crisis in 1973.

In addition to gaseous diffusion plants, French technology developed porous membranes by using various processes including extrusion of finely powdered metals/metal oxides (e.g. nickel and alumina), etching with a strong acid (e.g. gold-silver

alloys), and anodic oxidation (e.g. alumina). Oxide materials such as alumina and zirconia have drawn attention on account of their corrosion resistance toward UF_6 (Hsieh 1996).

Nanofiltration (NF) is the most recent pressure-driven membrane separation process developed after microfiltration (MF), ultrafiltration (UF), and reverse osmosis (RO). Its development dates back to late 1970s as a derived form of RO membrane with decreased separation performance for monovalent ions. However, since the term NF hadn't come into use at that time, it was classified as loose RO, intermediate RO/UF, or tight UF membrane. NF term seems to have been first used by FilmTec Co. (now a subsidiary of The Dow Chemical Company) in the mid-1980s (Jye and Ismail 2016).

2.2. Classification of Inorganic Membranes

Inorganic membrane classification generally is conducted based on materials structural properties. It can be possible to divide inorganic membranes into two main groups with respect to their pore size and structure.

2.2.1. Structure Based Classification

The main classes of membrane structures are dense and porous membranes. Metallic membranes (e.g. palladium, silver and their alloys), and solid electrolyte membranes (e.g. β-alumina, ZrO_2-Y_2O_3, and $RbAg_4I_5$) are examples of dense membranes. Porous membranes are made up of a porous wall or intermediate layers with micro/mesoporous top layers on a macroporous support.

The simplest form is a single and uniform wall of a fixed material which is known as symmetric membranes. Symmetric membranes require considerable thickness in order to acquire acceptable mechanical strength. Large thickness requirement of symmetric membranes is likely to have a negative effect on membrane fluxes (Burggraaf 1996). Since thin separation layers are needed in order to achieve high fluxes, the most widely used membranes in separation processes have an asymmetric structure. A cross-sectional SEM image of a porous asymmetric-composite ceramic membrane is shown in Figure 2.1. It is clearly seen that this asymmetric membrane structure consists of a single intermediate layer on a porous support and a thin dense separation top layer on this intermediate layer.

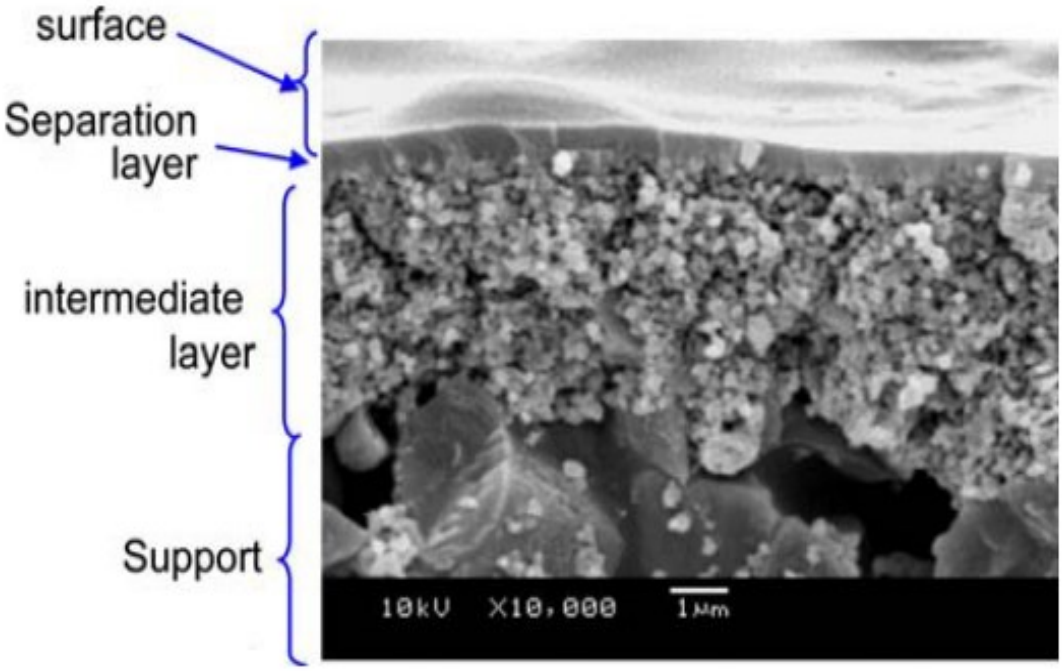

Figure 2.1. A cross-sectional SEM image of asymmetric-composite ceramic membrane (Source: Tsuru, 2008).

2.2.2. Pore Size Based Classification

Pressure-driven membranes can be classified into four groups based on their pore sizes: microfiltration, ultrafiltration, nanofiltration, and reverse osmosis. Basic properties of these membranes are listed in Table 2.1. Bacteria, turbidity, and suspended particles can be removed by microfiltration membranes. Ultrafiltration membranes typically remove colloids, polysaccharides, emulsified oils, and several viruses and bacteria. Organic compounds and multivalent ions can be removed by nanofiltration. Almost all impurities including monovalent ions can be retained by reverse osmosis (Shareefdeen et al. 2015).

A schematic diagram of membrane pore sizes achieved by using different materials is shown in Figure 2.2. The α-alumina phase has superior stability in a wide pH range but is limited to the microfiltration range due to the relatively larger pore sizes formed during high temperature processing. Although γ-alumina is reported to have a suitable pore size in the ultrafiltration range it is not as stable as α-alumina. The recent interest on research and applications of titania and zirconia membranes with pore sizes in

Table 2.1. Fundamental properties of pressure-driven membrane filtration types (Source: Shareefdeen et al., 2015).

Filtration type	Particle size removed	Contaminants removed	Pressure ranges
Microfiltration (MF)	0.1-10 µm	Suspended solids, bacteria, protozoa	1-3 bar
Ultrafiltration (UF)	10-100 nm	Colloids, polysaccharides, proteins, most bacteria, virus (partially)	2-10 bar
Nanofiltration (NF)	1-10 nm	Viruses, organic species, multivalent ions	6-10 bar
Reverse osmosis (RO)	0.1-1 nm	Monovalent ions	10-70 bar

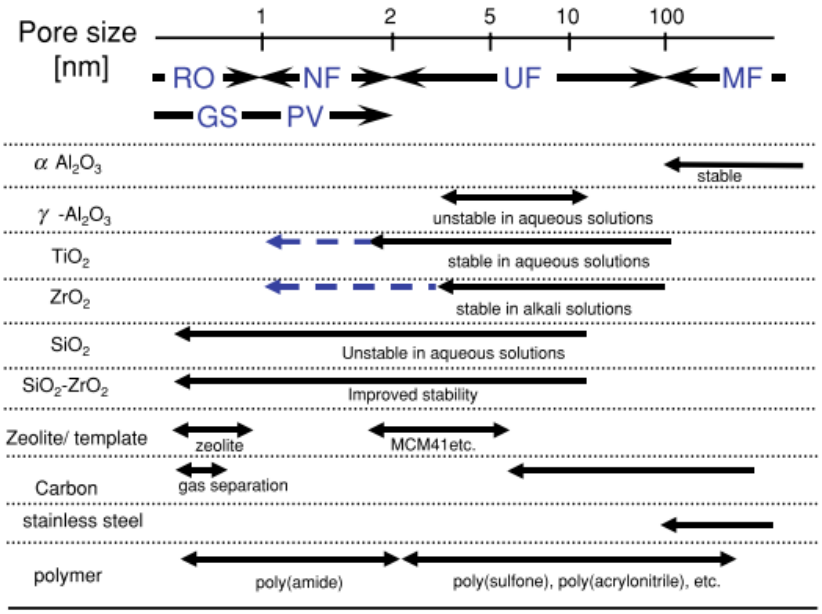

Figure 2.2. Pore size ranges of porous membranes made up of different materials (Source: Tsuru, 2008).

the nanofiltration range is mostly due to their excellent chemical stability. The pore size of amorphous silica can be easily controlled even in the RO range but it is unstable in aqueous solutions (Tsuru 2008).

Table 2.2. Various applications of pressure-driven membrane processes.

Filtration type	Application
Microfiltration (MF)	Whey separation, biomass separation, pretreatment to UF, NF, and RO
Ultrafiltration (UF)	Uranium enrichment, fruit juice clarification milk and whey processing, alcohol recovery, purification of pharmaceuticals, germ separation, oil/water separation
Nanofiltration (NF)	Surface water treatment, groundwater treatment, wastewater treatment, desalination, demineralization.
Reverse osmosis (RO)	Desalinating seawater, food & beverage, electronics

Potential applications of membranes are primarily determined by the pore size. Table 2.2 shows various applications of pressure-driven membrane processes. MF membranes are generally used in food industry and for the pretreatment of UF, NF and RO membranes. UF membranes have been used for various applications from uranium enrichment to biological separations. NF membranes are generally utilized for water softening, desalination and demineralization applications. Another important application of NF membranes is the pretreatment of saline waters to reduce the RO membrane fouling problems. RO membranes are often used in seawater desalination and food & beverage industries.

CHAPTER 3

SOL-GEL BASED CERAMIC MEMBRANES

Asymmetric porous ceramic membranes are generally formed from a macroporous support which is mainly responsible from mechanical strength and a number of thin selective layers on the support surface with the necessary separation abilities. The tubular supports are generally made from α-Al_2O_3 or TiO_2 by extrusion.

The production of defect-free (absence of cracks and pinholes) selective layers with high separation performance/abilities and homogeneous thicknesses and narrow pore size distributions is the most important concern in ceramic membrane processing. The preparation of stable colloidal sols of nanometer sized particles/species is necessary for the fabrication of these selective layers.

The sol-gel process is the most commonly used and suitable method for the preparation of these meso/microporous ceramic selective membrane layers. There are many factors affecting sol-gel chemistry (i.e. type of precursors, hydrolysis ratio, solvent type/concentration, catalyst type/concentration, dopant type/concentration etc.). The nanostructure of membranes can be tuned by optimizing the sol size/structure, drying and heat treatment conditions. Fabrication of ceramic membranes is a very delicate process where a large number of parameters that must be closely controlled.

3.1. Sol-Gel Routes

Sol-gel processes involve hydrolyzation of inorganic or metal-organic precursors and condensation/polymerization reactions resulting in the development of colloids and clusters at the same time. There are two routes in the sol-gel process which are the colloidal and polymeric routes. A schematic diagram of colloidal and polymeric sol-gel routes for ceramic membrane preparation is given in Figure 3.1. Colloidal sol-gel route depends on colloid chemistry in aqueous media, whereas polymeric sol-gel route is related to the chemistry of metal organic precursors in organic solvents (Guizard 1996). In the colloidal sol-gel route, both hydrolysis and condensation reactions are fast resulting in a fully hydrolyzed alkoxide (highly branched polymer). In the polymeric sol-gel route,

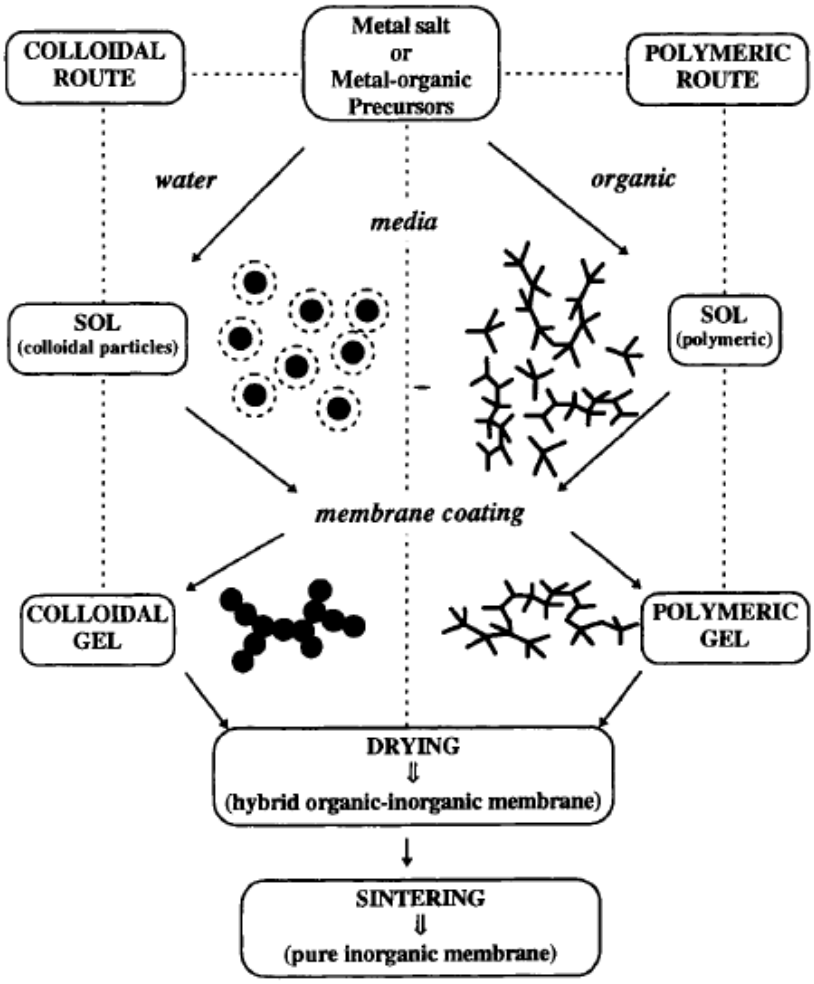

Figure 3.1. Diagram of inorganic membrane preparation by colloidal and polymeric sol-gel routes (Source: Guizard, 1996).

a slow hydrolysis reaction occurs due to the small amount of water addition which results in a partial hydrolyzation of alkoxide (linear inorganic polymer) (Tsuru 2008).

3.2. Sol-Gel Chemistry and Interrelated Parameters

Two main reactions occurring in sol-gel processing (hydrolysis and condensation) are illustrated in Figure 3.2. Metal alkoxides react readily with water. This substitution reaction is called hydrolysis since hydroxyl ion becomes linked to the metal atom (Brinker and Scherer 1990). Hydrolysis is also defined as the deprotonation of a solvated metal cation. Proton loss takes place by the water molecule(s) which surrounds the metal in the first solvation shell. Solvation of a cation and an anion are illustrated in Figure 3.3. The

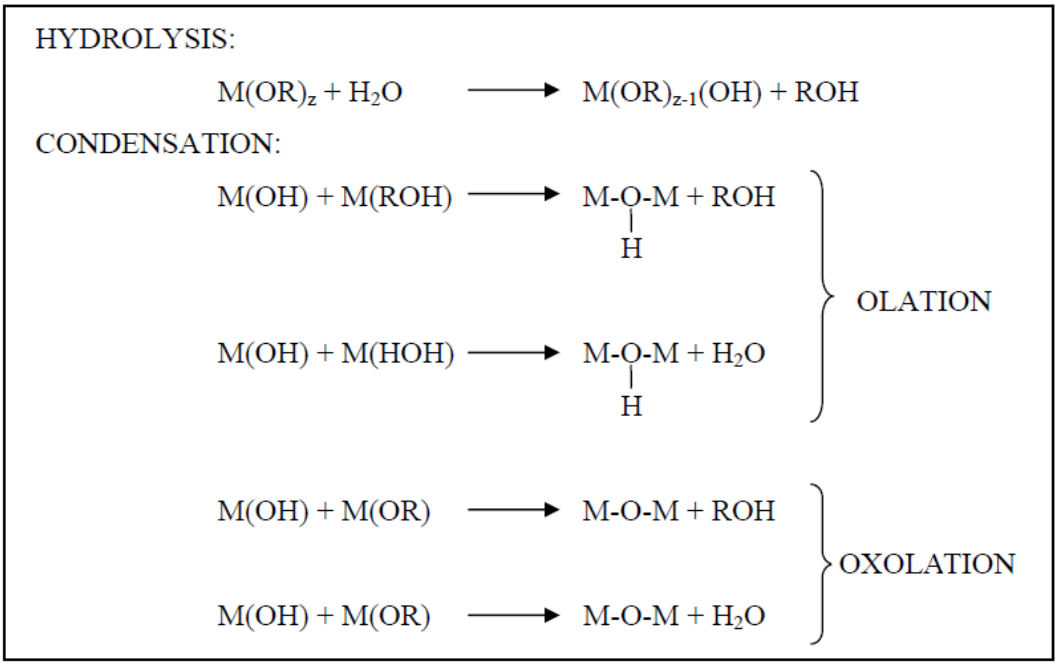

Figure 3.2. Simultaneous reactions in sol-gel processing (M: metal, R: alkyl group) (Source: Erdem, 2009).

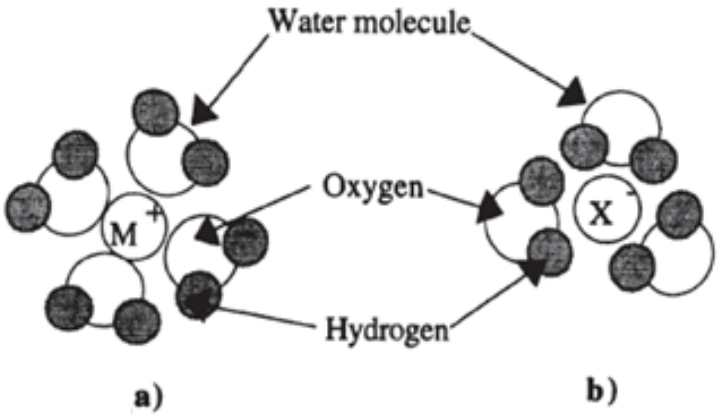

Figure 3.3. Solvation of a) a cation and b) an anion (Source: Pierre, 1998).

solvation of cations is responsible for the hydrolysis of precursors, therefore it is much more important compared to that of anions (Pierre 1998).

Condensation is a polymerization reaction which leads to the formation of a polynuclear complex consisting of two metal atoms from two mononuclear complexes of M. The condensation is responsible for the formation of "ol" and "oxo" bridges which are named as olation and oxolation, respectively (Figure 3.2). Further information on sol-

gel reaction mechanisms is given elsewhere (Livage et al. 1988, Brinker and Scherer 1990, Pierre 1998).

Reactivity of a precursor has to be low in order to control hydrolysis and condensation reactions. Metal alkoxide reactivity strongly depends on electronegativity or degree of unsaturation. The hydrolysis rate of a metal alkoxide is also inversely proportional to the size of the alkyl group due to the fact that partial positive charge of metal ions decreases with alkyl chain length and steric hindrance effect. Hydrolysis rate usually decreases in the following order: ethoxide>propoxide>butoxide and tertiary>secondary>primary.

Hydrolysis ratio is defined as the molar ratio of water to metal alkoxide. Membrane nanostructure can be tailored by changing this ratio. The complete hydrolysis of titanium tetraisopropoxide (TTIP) stoichiometrically necessitates a hydrolysis ratio of two. Polymeric species can be obtained by using a hydrolysis ratio close to the stoichiometric amount.

Solvents are often used to homogenize the metal alkoxides with the other reactants to prepare an appropriate media for hydrolysis. Formation of oligomers rather than monomers is favorable which can be supplied by dilution. Nevertheless, solvents are not chemically inert which makes solvent type and amount an important parameter in sol-gel processing. Size and chemical polarity of solvent control the rate of hydrolysis and condensation and therefore the microstructure of the membrane layer (Topuz 2009). Catalyst type and pH are the other important factors affecting the kinetic growth models and the morphology by changing the gel microstructure (Brinker and Scherer 1990).

Type of dopants is another critical parameter in sol-gel processing. The XRD data on lanthana (La_2O_3) or yttria (Y_2O_3) doped TiO_2, ZrO_2 or Al_2O_3 membranes indicated only the anatase phase of titania, the tetragonal phase of zirconia and the γ-Al_2O_3 phase of alumina and no dopant oxide phases. The dopant oxide either was claimed to be located in the grain boundaries or integrated into the lattice structure of the main phase (Lin et al. 1994). The effects of rare earth (RE) nitrate doping in sol-gel derived titania nanostructure evolution was investigated in a recent work. The rare earth ions were concluded to be either in the domain boundaries or partially in the interstitials of the amorphous dried gel structure. These RE ions reacted with the main phase and formed RETiO phases in the grain boundaries during heat treatment as schematically shown in Figure 3.4 (Yurtsever and Çiftçioğlu 2017).

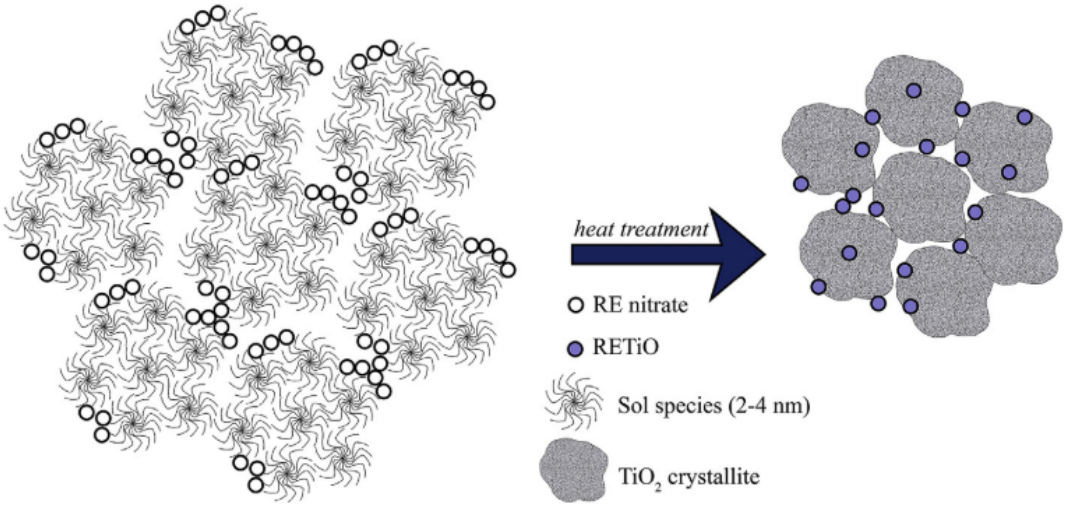

Figure 3.4. Schematic representation of proposed nanostructure evolution in rare earth nitrate doped titania (Source: Yurtsever and Çiftçioğlu, 2017).

3.3. Sol-Gel Film Formation

The evolution of sols and gels heavily depend on the nature of the precursor in sol-gel processing of ceramic membrane selective layers. Two different gel layer structures form based upon the sol-gel route used: colloidal gels which are predominantly formed by steric or electrolytic effects, and polymeric gels in which relative rate and extent of reaction are important.

The reasons for the coating of one or more layers on a porous support are to decrease the average pore size, surface roughness, and void/defect density. Porous ceramic layers on the porous support are generally prepared by dipping into a ceramic suspension for a set time interval. This is followed by the withdrawal at a certain rate from the suspension. This commonly used method for the formation of porous ceramic layers on extruded porous tubes is called as “dip-coating” or “withdrawal coating”. Ceramic layers can also be prepared by pressure filtration of sol using the support or former layer as a filter (Bonekamp 1996).

Two different consolidation/packing modes exist during the withdrawal of tubes from a sol: capillary filtration and film-coating. Capillary filtration takes place when dry tube surface is wetted by the sol and capillary forces drive particles to the interface. The

particles in the suspension/sol consolidate at the solid/liquid interface forming a dense gel. The sizes of the pores present in the solid surface must be small enough for the

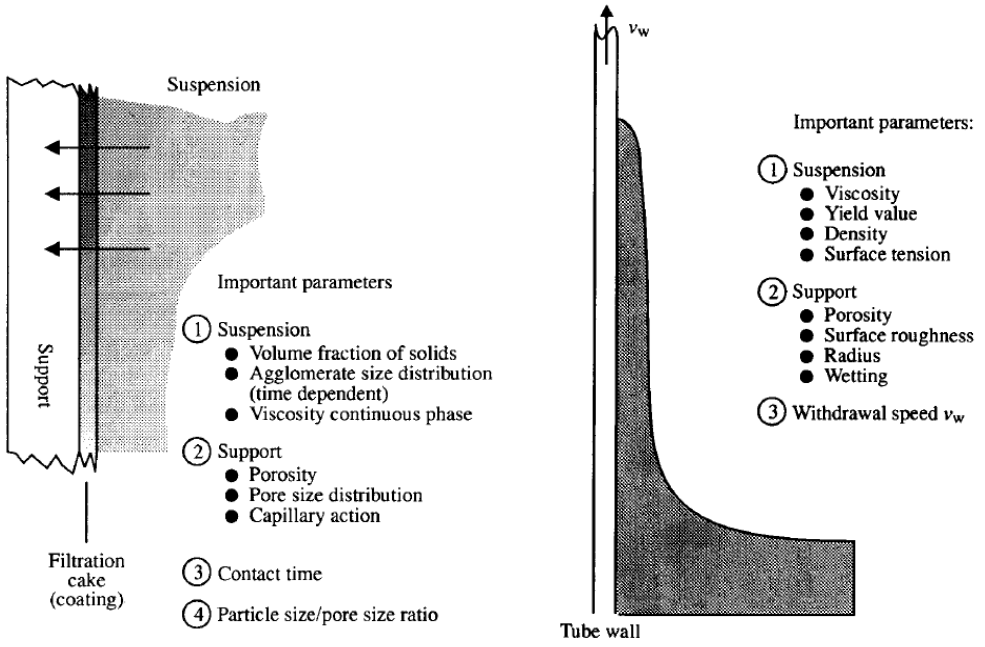

Figure 3.5. Mechanism and important parameters in the a) capillary filtration, b) film-coating mode of dip-coating (Source: Bonekamp, 1996).

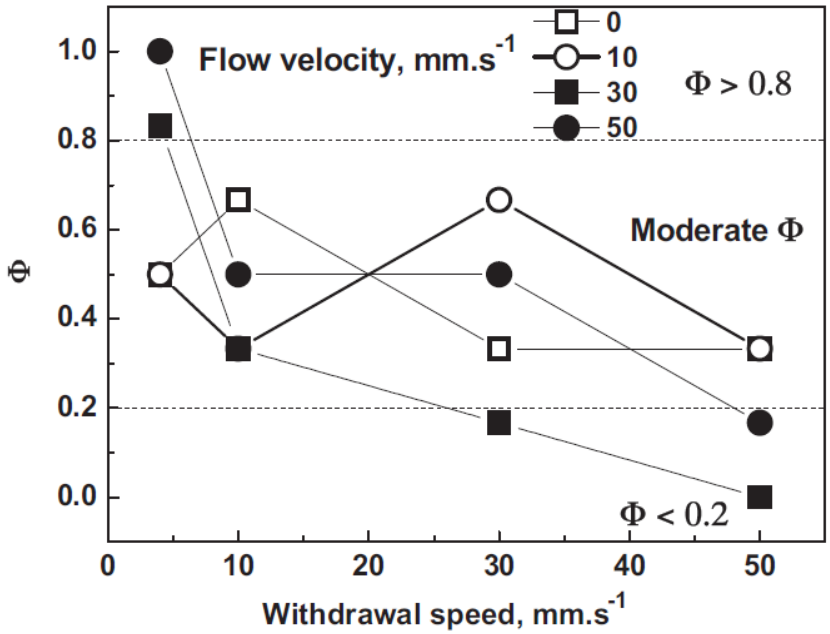

Figure 3.6. Influence of flow velocity and withdrawal speed on the probability of pinhole avoidance (Source: Zhu et al., 2011).

prevention of sol particle/species impregnation (Bonekamp 1996). Capillary filtration and film-coating modes of dip-coating and the related most important parameters are summarized in Figure 3.5.

A modified dip-coating method in the capillary filtration mode for the formation of defect-free MF layers was proposed recently (Zhu et al. 2011). The importance of the withdrawal speed along with flow velocity of the suspension in the tubular support can be seen in Figure 3.6 where the closeness of ϕ to 1 indicates defect-free MF layer formation.

CHAPTER 4

CERAMIC NANOFILTRATION TOP LAYERS

Many researchers have prepared nanofiltration membranes using different ceramic materials over the last two or three decades. These materials are mainly titania, zirconia, silica, alumina and their mixed-oxide forms. These nanofiltration membranes were characterized by using various techniques including filtration performance experiments in order to determine and optimize the NF membrane performances/separation capacities.

4.1. Titania NF Membranes

Puhlfürß et al. (2000) developed microporous TiO_2 nanofiltration membranes by a polymeric sol-gel route. These membranes were coated on tubular supports with a multilayer structure. The top layer of this multilayer structure was a mesoporous TiO_2 layer with 5 nm mean pore size and a thickness of 250 nm. They claimed that at high humidity reaction rate of hydrolysis was greater than that of condensation causing the formation of TiO_2-xH_2O particles and mesoporous interparticle pores. Polymeric gel layers were consequently formed and dried under controlled conditions (humidity <50% and temperature=22°C) and finally heat treated at 450°C. The resulting pure water permeability and molecular weight cut-off values were determined as 20 L/(m^2 h bar) and 480 Da, respectively which is graphically given in Figure 4.1. The pure water permeability was almost time independent as shown in Figure 4.1a. The PEG retention levels were slightly increased from 2 to 4 bar transmembrane pressure (TMP) at low molecular weights whereas MWCO values were found to be nearly the same as seen in Figure 4.1b.

Multichannel α-alumina supports with intermediate layers were coated with TiO_2 sols in another work on nanofiltration membranes (Voigt et al. 2003). The results of MWCO determination experiments with 0.5% aqueous PEG solution with three different membranes are given in Figure 4.2. Type 1 membranes were coated with 1.0 wt% TiO_2 sol prepared by partial hydrolyzation of titanium isopropoxide with isopropyl alcohol.

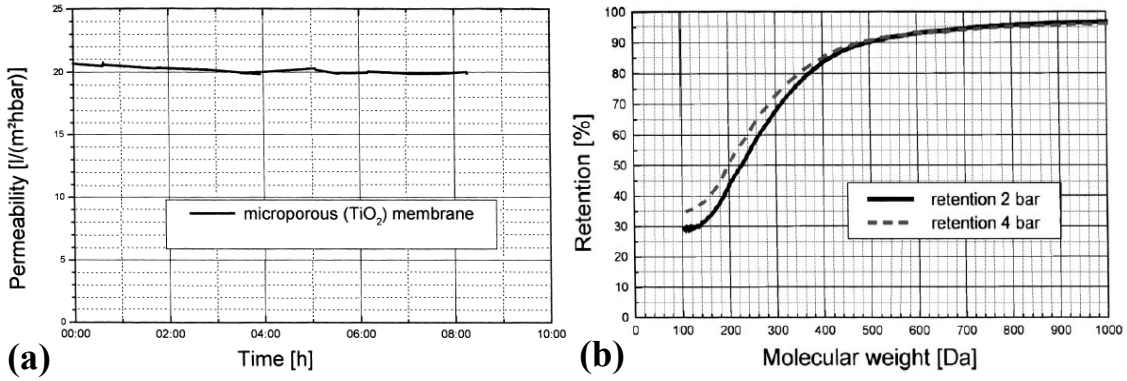

Figure 4.1. Microporous TiO_2 NF membrane a) pure water permeability at 6 bar b) PEG retention at 2 and 4 bar (0.5 wt% PEG) (Source: Pühlfürß et al., 2000).

Type 2 membranes were coated with the dilution of the first sol from 1.0 wt% sol to 0.2 wt% with isopropyl alcohol. Type 3 membranes were prepared by coating Type 2 membrane with diluted unhydrolyzed titanium isopropoxide. The results of this work supports the use of successive NF coatings for the reduction of the extent of defects/microcracks present in the NF layers which reduces the MWCO values enhancing separation capacity. The use of unhydrolyzed TTIP for the final layer (where hydrolsis was completed by atmospheric moisture) formed a NF layer with a very narrow MW vs. Retention distribution.

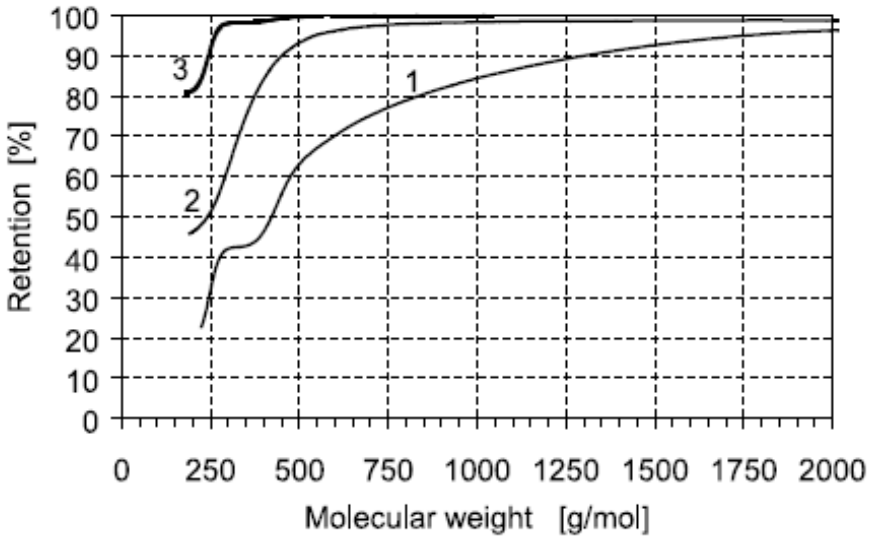

Figure 4.2. PEG retentions of three different NF membrane sol types at TMP=3 bar (Source: Voigt et al., 2003).

4.2. Zirconia and Alumina NF Membranes

ZrO_2 and TiO_2 NF membranes were produced via a polymeric sol-gel technique by Benfer et al. (2001). These ZrO_2 and TiO_2 NF membranes were prepared on tubular membranes with UF layers of similar oxides. These NF membrane layers were produced by pouring polymeric sols into tubular supports (TiO_2 NF layers were coated on TiO_2 UF layers, and ZrO_2 NF layers were coated on ZrO_2 UF layers). The capillary suction of sol solvent resulted in an accelerated condensation reaction on the inner surfaces of the substrates. The gel layers dried at room temperature for 3 days were further heat treated/pyrolyzed at 500°C to form the membrane layer. Pore size distributions of these TiO_2 and ZrO_2 NF membranes are given in Figure 4.3a. Smaller pores and narrower pore size distributions were observed in the ZrO_2 NF membranes. The variation of the relatively high fluxes of these membranes with time is also given in Figure 4.3b. The flux of the ZrO_2 NF membrane with smaller pores is significantly lower than the TiO_2 NF membrane. The feed to the cross-flow filtration experiments was a dye containing solution which caused fouling of the membranes.

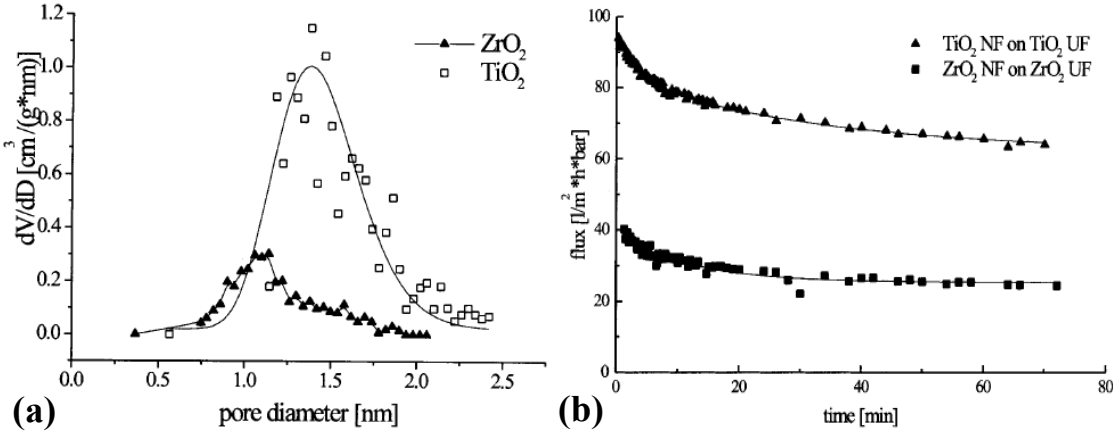

Figure 4.3. Microporous TiO_2 and ZrO_2 NF membrane (a) pore size distribution by mercury porosimetry method, (b) permeation flux during 'Direct red MW=990.8 g/mol' cross-flow filtration (Benfer et al., 2001).

Schaep et al. (1999) produced γ-Al_2O_3 membranes by coating boehmite sol on α-Al_2O_3 support discs. The preparation of these membrane with highest separation performance was performed in two steps. The first step was the coating of a boehmite sol with a low amount of PVA to avoid crack formation and applying heat treatment at 600°C.

The second layer was coated with a boehmite sol without PVA and heat treated at 400°C. This membrane eventually had a MWCO value of 900 Da and a clean water permeability value of 2.3 L/(m^2 h bar).

4.3. Mixed-Oxide NF Membranes

In a pioneering study by Aust et al. (2006) on unsupported TiO_2-ZrO_2 mixed-oxide membranes sols were dried and an XRD analysis was conducted in order to determine the crystallization behavior as a function of composition and heat treatment temperature. The resulting crystallization temperature ranges for different TiO_2-ZrO_2 compositions can be seen in Figure 4.4. Mixed-oxide membranes crystallize at relatively higher temperatures in the 30-60 mol% ZrO_2 range which may have very valuable implications on defect-free NF layer formation by minimizing crack/defect formation due to shrinkages experienced by the NF layer during the unavoidable heat treatment stage.

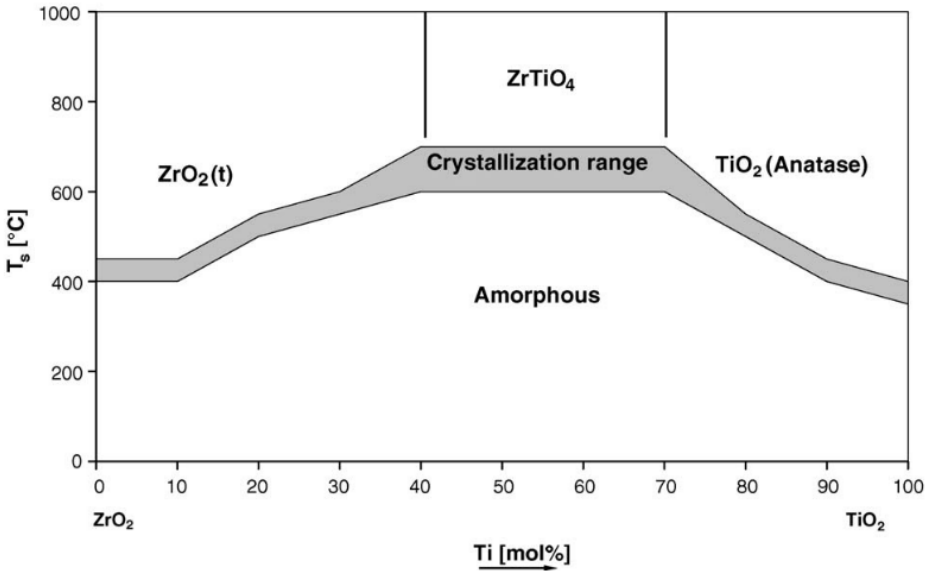

Figure 4.4. Crystallization behavior of TiO_2-ZrO_2 mixed-oxide NF membranes (Source: Aust et al., 2006).

TiO_2-ZrO_2 mixed-oxide NF membranes via polymeric sol-gel method were also formed on tubular α-alumina supports with TiO_2-ZrO_2 mixed-oxide intermediate layers which were prepared using a colloidal sol-gel route. These intermediate UF layers

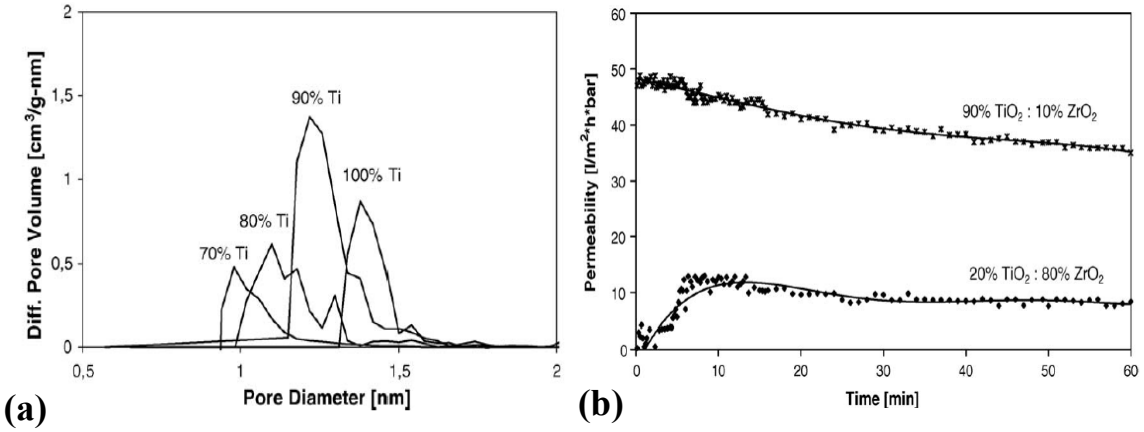

Figure 4.5. Microporous TiO_2-ZrO_2 NF membrane (a) pore size distribution by mercury porosimetry method with as a function of titania content, (b) permeation flux during 'Direct red MW=990.8 g/mol' cross-flow filtration (Source: Aust et al., 2006).

were used as substrates to be coated with polymeric sols. Tetraethyl orthotitanate and zirconium (IV) propoxide (ZTP) were used as metal alkoxide precursors and diethanolamine as chelating agent in the preparation of the polymeric sols. The inner surfaces of these membranes were dip-coated for 1, 5 or 10 minutes and the remaining sols were poured off the tubular membrane. These membranes were heat treated at 450°C or 500°C. The pore diameters and cross-flow permeation fluxes of the NF membranes during Direct-red filtration are reproduced presented in Figure 4.5. The pore diameters of these NF membranes decrease with increased zirconia content as seen in Figure 4.5a. The permeation flux of the titania-rich mixed-oxide NF membranes during Direct-red filtration was recorded to be significantly higher than that of the zirconia-rich membranes as seen in Figure 4.5b.

CHAPTER 5

EXPERIMENTAL

5.1. Materials

Tubular ceramic membrane supports were prepared by using α-alumina powders with average particle sizes of 5.2, 1.3, and 0.5 μm (CL 4400 FG, CT 1200 SG, CT 3000 SG, Almatis), boehmite powder (Disperal, Sasol), hydroxypropyl methylcellulose (HPMC, Methocel F4M, The Dow Chemical Company), glycerin (Dalan Kimya), and deionized water.

MF layers were formed by using two different alumina powders which were 0.5 μm (CT 3000 SG, Almatis) and 0.18 μm (AKP-50, Sumitomo), polyvinyl alcohol (PVA, Aldrich 80% hydrolyzed) (M_w = 9000-10000 g/mol), dispersant (DOLAPIX CE 64), defoamer (Dağlar Kimya A.Ş) , and deionized water.

The first UF layer was formed by using disperal (crystallite size=10 nm and BET surface area=180 m^2/gr as supplied by the company) boehmite powder, nitric acid (Merck 65%), PVA (80% hydrolyzed, M_w = 9000-10000 g/mol), and deionized water. The second UF layer was formed by using P2 (crystallite size=4.5 nm and BET surface area=260 m^2/gr as supplied by the company) boehmite powder and deionized water. The third UF layer was formed by using titanium (IV) butoxide (TTB, Aldrich 97%), glycerin (Dalan Kimya), nitric acid (Merck, 65%), and deionized water.

Titanium (IV) isopropoxide (TTIP, Aldrich 97%), zirconium (IV) propoxide (ZTP, Aldrich 70%), neodymium (III) nitrate hexahydrate ($Nd(NO_3)_3.6H_2O$, Aldrich 99.99% trace metal basis), nitric acid (Merck, 65%), deionized water, ethanol (Merck), and 1-propanol (Merck) were the chemicals used in the preparation of the supported and unsupported selective NF membranes.

Molecular weight cut-off (MWCO) experiments were performed using aqueous polyethylene glycol (PEG, Aldrich) solutions. PEGs with different molecular weights (400, 1000, 2000, 10000, 20000 Da) were used in this characterization.

5.2. Methods

The MF, UF and NF layers were coated on porous tubular alumina supports extruded in our laboratory in a successive manner. The film formation on the inner surface of the support by capillary suction forces was simply conducted by pouring the suspension into the tubes from one end while sealing the other with parafilm. The parafilm was punctured to withdraw the remaining sol at a slow withdrawal rate after a preset dip-coating time. This coating technique was used for the formation of all layers by varying the dip-coating time. Sols and unsupported membranes were characterized in order to gain a better understanding of the selective layer nanostructures. MWCO characterizations and flux determinations were performed in a cross-flow filtration set up.

5.2.1. Preparation of Tubular Ceramic Supports

Support preparation is a prerequisite for the preparation of separation layers since the support structure serves as a substrate providing mechanical stability for the relatively thin selective layers. In this study, tubular ceramic membrane supports (L: 200 mm, ID/ OD: 16/25 mm) were prepared by piston extrusion. The flowchart of tubular alumina membrane support preparation process is given in Figure 5.1. Tubular ceramic membrane production steps are dry mixing in ball mill, pre-kneading by hand, kneading, extrusion, drying on tube roller overnight, drying in an oven at 90°C, removal of binders from the body (debinding) at 250-350°C, and sintering at 1525°C for 2 hours, respectively.

5.2.2. Preparation of Microfiltration Layers

The MF layers are needed in order to minimize the number of defects inevitably formed during the processing of tubular supports and forming a dense defect-free layer on the inner surface where relatively thin crack/pinhole free UF and NF layers can be formed. The preparation route of MF membrane layers is given in Figure 5.2 which starts with the preparation of a stable well dispersed α-alumina suspensions (7 wt%).

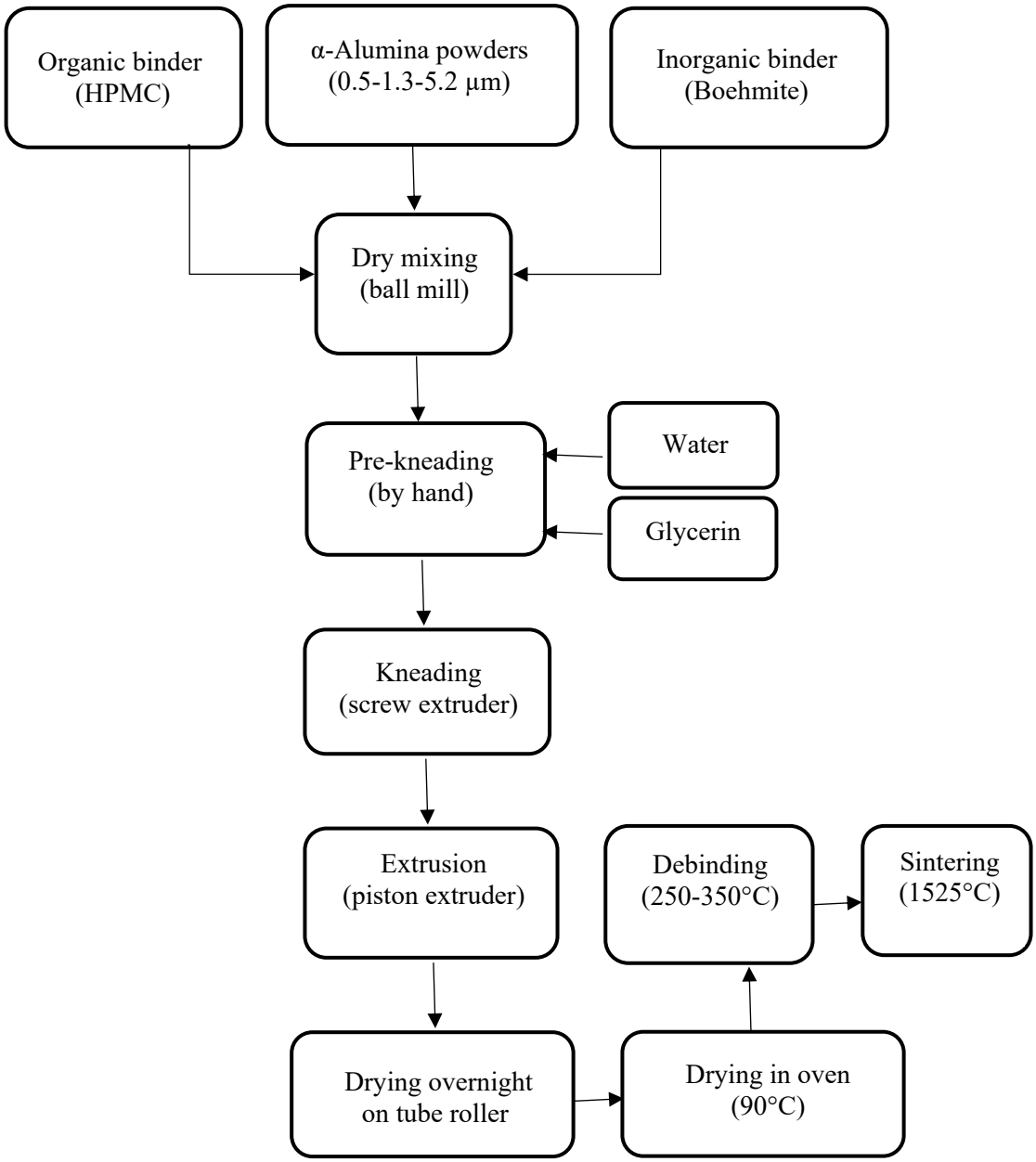

Figure 5.1. Flowchart of tubular α-alumina membrane support preparation.

The dispersion medium (water) was heated to 70°C in order to dissolve the binder/drying control additive (PVA 3 wt%). The alumina powder was dispersed by adding dispersant under constant magnetic stirring. A defoaming agent was also added in order to eliminate the gas bubbles formed due to the PVA addition and the dispersion was ultrasonically treated in an ultrasonic bath for couple of hours for complete deagglomeration of the powders. The tubes were dip-coated with the prepared well dispersed stable suspension with a coating time of 5 minutes and dried overnight in a vertical position. The dried tubes were finally heat treated in a high temperature muffle furnace (Carbolite CWF 1300).

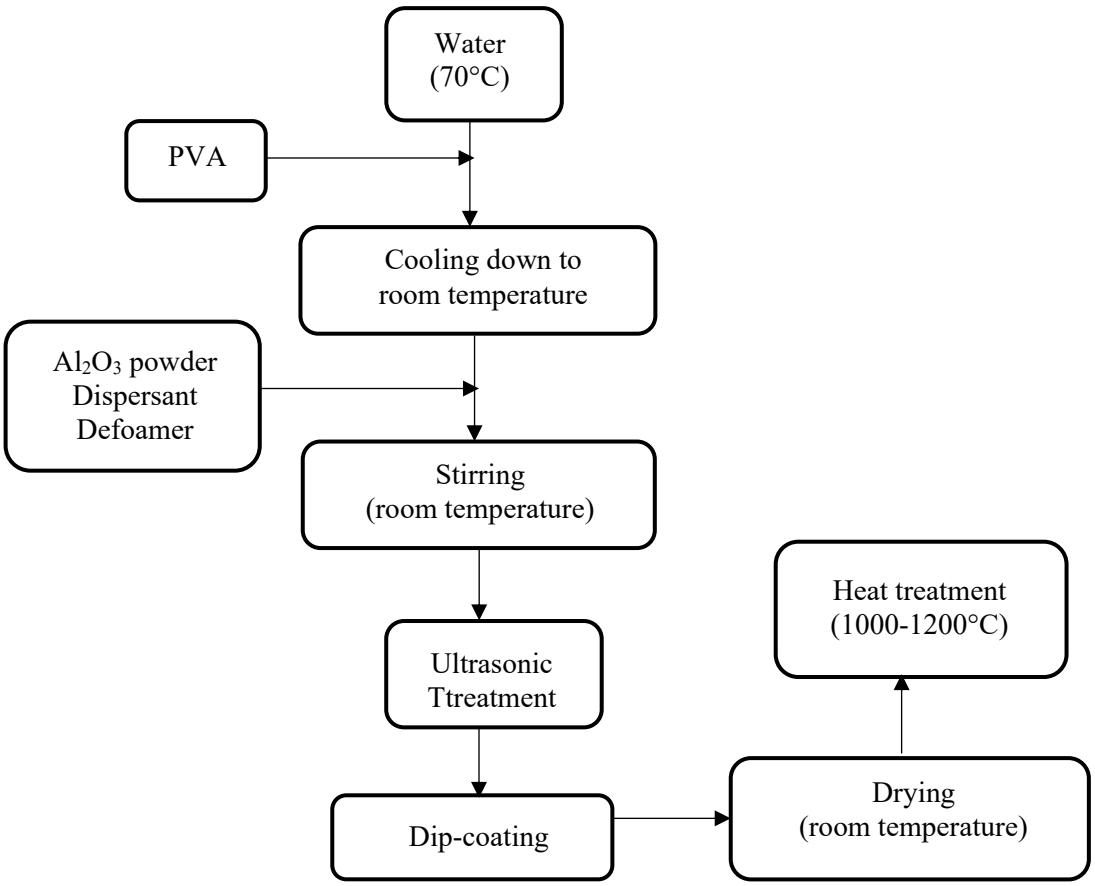

Figure 5.2. Preparation route of microfiltration membrane layers.

5.2.3. Preparation of Ultrafiltration Layers

Three different ultrafiltration membrane layers were prepared: the first two UF layers (γ-Al_2O_3) were prepared with disperal and P2 boehmite sols, and the third UF layer (TiO_2) was prepared with a titania hydrosol. Disperal boehmite sol was composed of 0.8 wt% of disperal powder, 0.25 wt% PVA, nitric acid, and deionized water (0.8 g of disperal boehmite powder, 0.25 g of PVA 3 mL of 1 M HNO_3 and balance water in 100 mL sol). Disperal boehmite powders were peptized by 20 minutes of stirring followed by 20 minutes of ultrasonic treatment. This procedure was repeated until a transparent bluish sol is obtained. The tubes which have been coated with microfiltration layers were coated with disperal sol for 10-20 seconds, and were dried at room temperature in a vertical position for 24 hours. The dried tubes were heat treated at 600°C in a high temperature furnace (Carbolite CWF 1300). A schematic representation of the preparation of the first ultrafiltration layer is given in Figure 5.3.

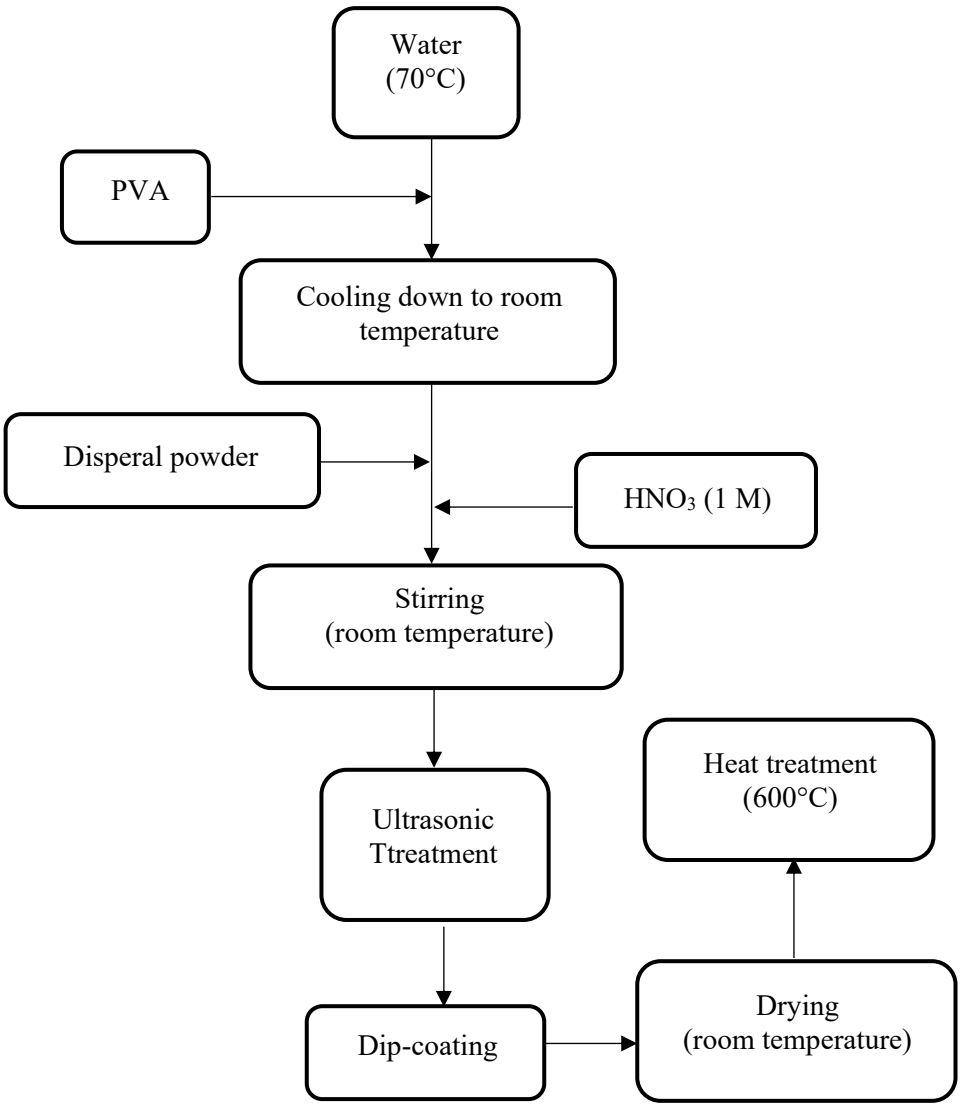

Figure 5.3. A schematic representation of the preparation of the first γ-Al_2O_3 UF layer.

P2 boehmite sol was prepared using 0.8 wt% P2 boehmite powder for the preparation of second γ-Al_2O_3 UF layer. A schematic representation of the preparation of second γ-Al_2O_3 UF layer is given in Figure 5.4. P2 boehmite powder was added to deionized water and stirred at room temperature. Peptization was performed by using the same procedure as the disperal boehmite sol except the addition of acid as the powder was readily acid treated. Dip-coating times and the heat treatment temperatures were also similar to that of the first UF layer.

Titania hydrosol was used for the preparation of the third UF layer. Preparation route of this colloidal sol was performed by using a modified procedure of Lu et al. (2016). A schematic represantation of TiO_2 UF layer preparation is shown in Figure 5.5.

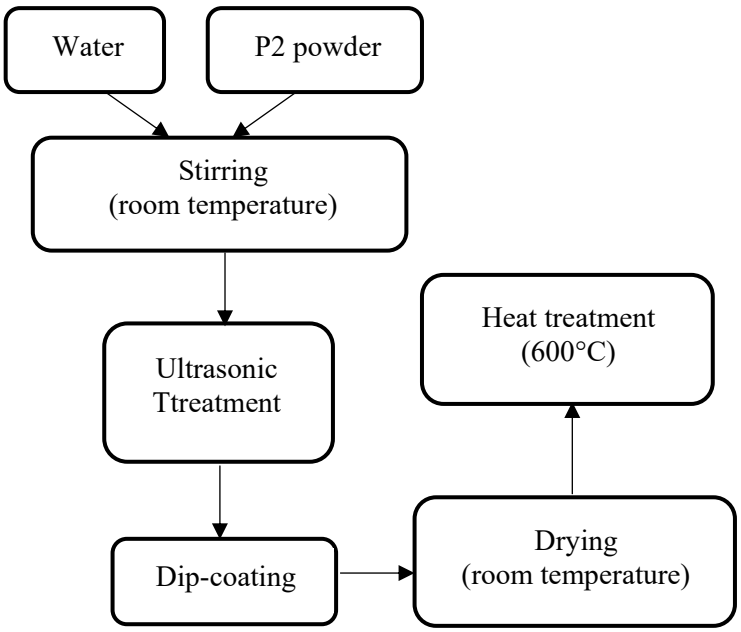

Figure 5.4. A schematic representation of the preparation of the second γ-Al_2O_3 UF layer.

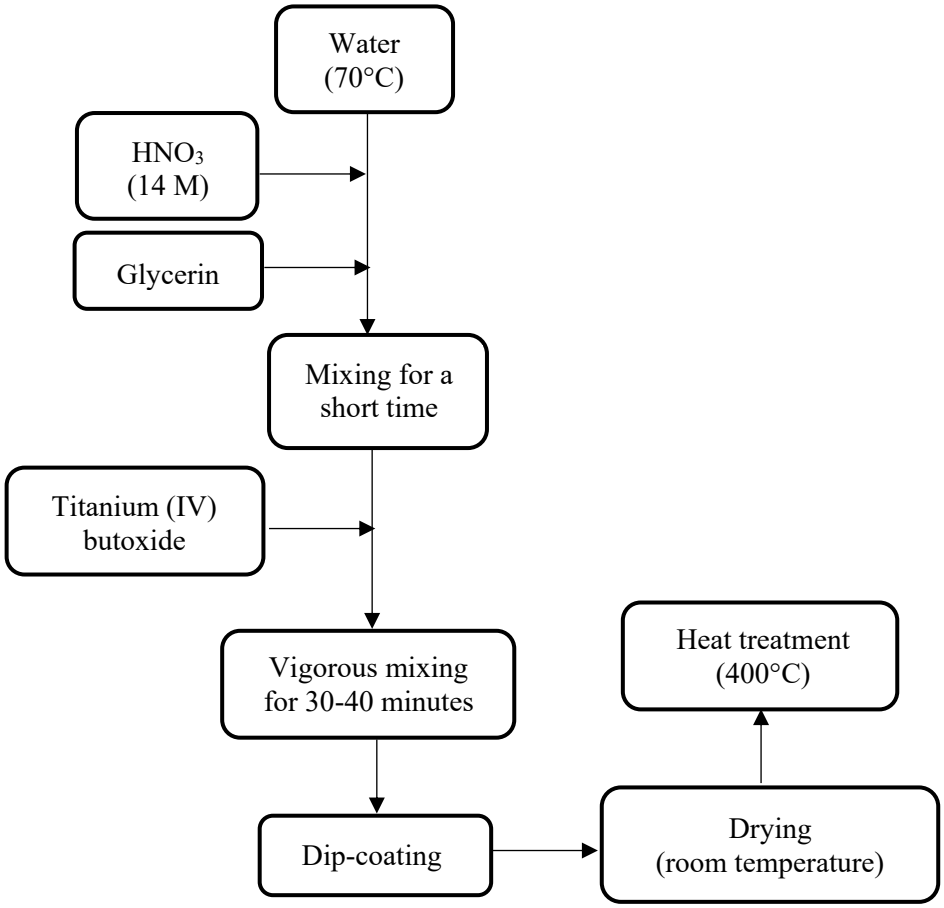

Figure 5.5. A schematic representation of TiO_2 UF membrane preparation.

Glycerin and nitric acid was added to the preheated water at 70°C. TTB was added dropwise after a homogeneous precipitant mixture was obtained. This mixture was stirred vigorously for 30-40 minutes and a transparent sol was obtained. Particle size distribution of the sol was determined by Zetasizer-DLS and finally dip-coating of the tubular membranes for 10-20 seconds were conducted. The dip-coated tubular membranes were dried in a vertical position at room temperature. The tubular membranes were finally placed in a muffle furnace and heat treated at 400°C.

5.2.4. Preparation of Nanofiltration Layers

Nanofiltration layers were prepared as both supported and unsupported membrane films. The unsupported membranes were prepared for the investigation of nanostructure evolution which may yield valuable knowledge towards the design of crack/defect-free subnano selective NF layers.

5.2.4.1. Preparation of Unsupported NF Layers

The consolidation behaviors, structural properties and their evolution during heat treatment of the actual selective NF membrane layers can only be understood by using the corresponding unsupported counterparts. Unsupported membrane films in the form of flakes were prepared by solvent removal/drying of the sols in a high surface area metal tray at room temperature. The thermal shrinkage/weight loss behaviors, phase/nanostructure evolutions, and crystallite sizes of these NF membrane powders/flakes were further investigated. A schematic representation of ZrO_2 mixed and neodymium doped polymeric sol production and unsupported TiO_2 NF membrane preparation and characterization is illustrated in Figure 5.6. The preparation route was similar to the supported NF membrane layer preparation except the use of ethanol as the solvent. A transparent sol with final molar TTIP+ZTP:H_2O:HNO_3:ethanol ratios of 1:2:0.053:52 was obtained with 3 wt% TiO_2 content in the preparation of unsupported NF layers.

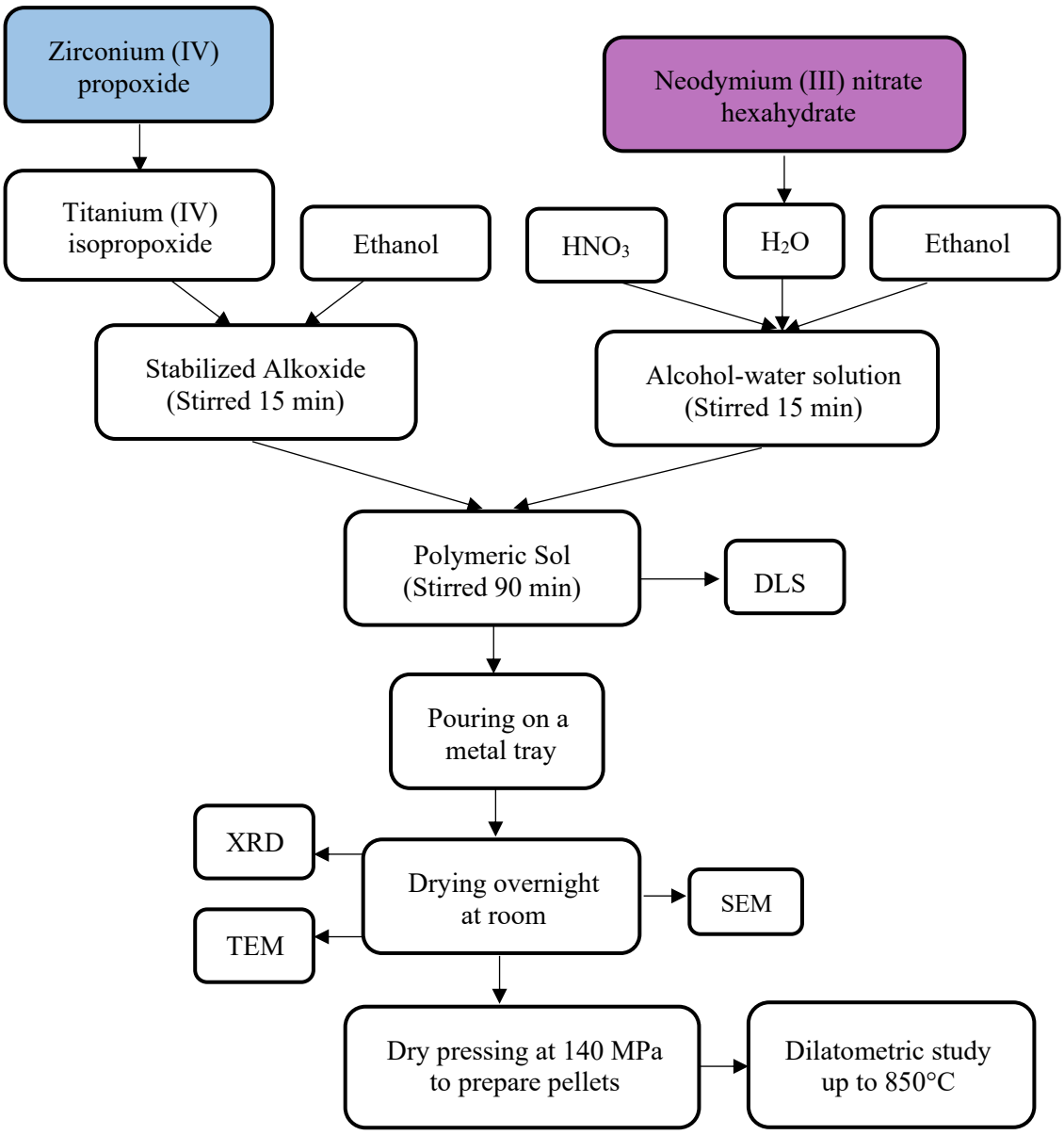

Figure 5.6. A schematic representation of ZrO_2 mixed and neodymium doped polymeric unsupported TiO_2 NF membrane preparation and characterization.

5.2.4.2. Preparation of Supported NF Layers

Neodymium doped and zirconia mixed TiO_2 layers were prepared by polymeric sol-gel technique using TTIP as titanium precursor. Neodymium (III) nitrate hexahydrate was used as a dopant precursor and zirconium (IV) propoxide was used as a precursor to be mixed with TTIP. The selective membrane sols were prepared by the dropwise addition of nitric acid, water, neodymium (III) nitrate hexahydrate and alcohol solution to the TTIP/(ZTP)/alcohol solution. A transparent sol with final molar

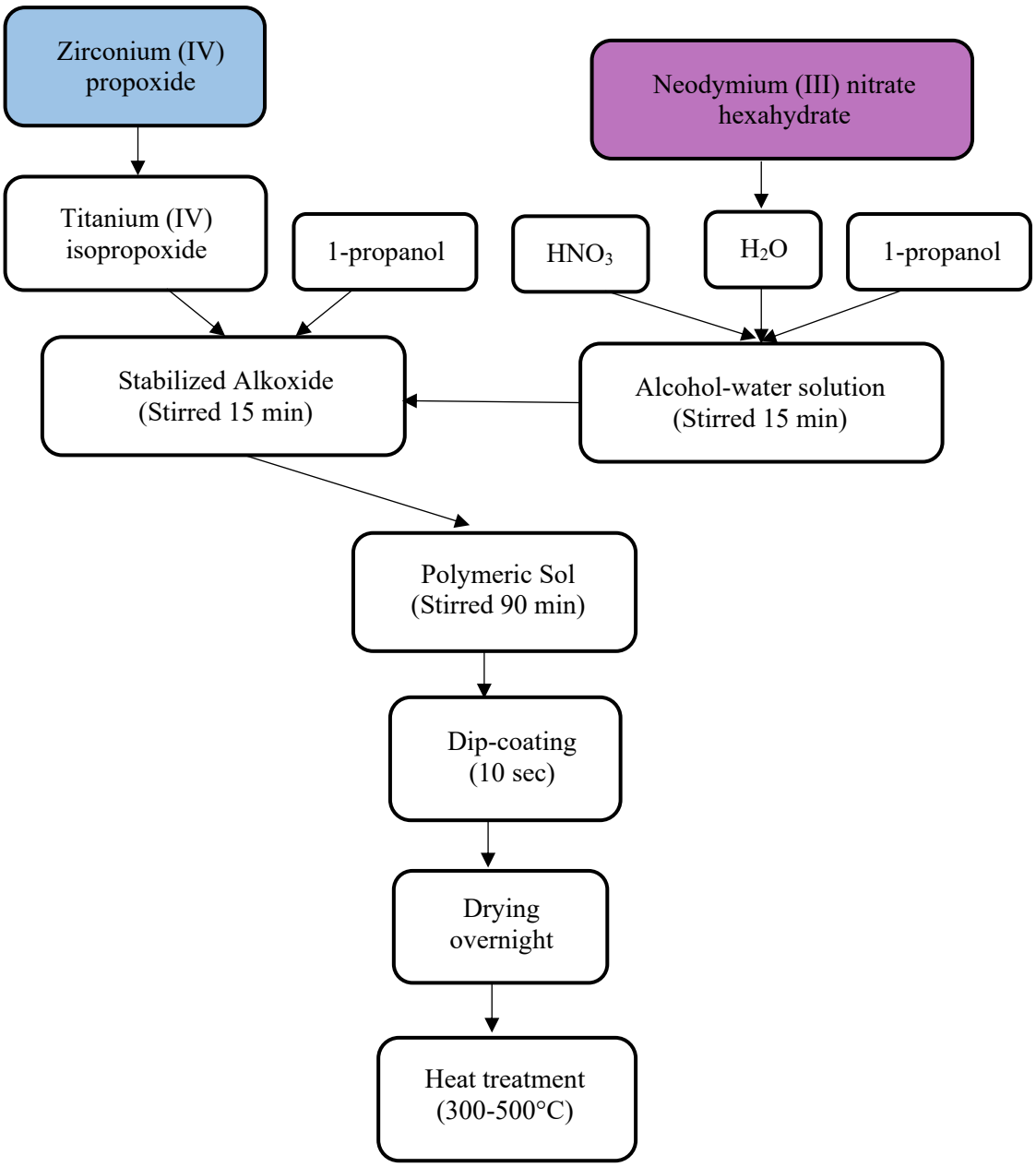

Figure 5.7. A schematic representation of ZrO_2 mixed and neodymium doped polymeric supported TiO_2 NF membrane preparation.

TTIP+ZTP:H_2O:HNO_3:1-propanol ratios of 1:2:0.053:138 was obtained with 1 wt% TiO_2 content after about 90 minutes of stirring at room temperature. The tubes which have been coated with TiO_2 UF layers were dip-coated with these polymeric sols, and were dried at room temperature in a vertical position for 24 hours. The coated tubes were finally heat treated between 300-500°C. A schematic representation of preparation of zirconium and neodymium doped polymeric TiO_2 NF layers is given in Figure 5.6.

5.2.5. Membrane Characterization

Sol particle sizes were determined by dynamic light scattering (DLS, Malvern Zetasizer 3000 HSA). Thermogravimetric behavior of unsupported membranes were determined by Shimadzu TGA51. The shrinkage/densification behavior of the unsupported membranes dry pressed at 140 MPa pressure (prepared pellets were approximately 5 mm in diameter and 4 mm in thickness) were determined by Linseis L76150B-1600 dilatometer. Dilatometric characterization was conducted from room temperature to 850°C with a heating rate of 2°C/min.

X-ray diffraction characterization was performed by Philips X'Pert Pro equipment with monochromated high-intensity CuKα (λ=1.54Å) radiation in order to determine the phase transformation temperature ranges. Scan range was kept between 5°-80° with 0.033° step size.

The anatase crystallite sizes were calculated from the broadening of the (101) reflection using Scherrer's equation:

$$D = \frac{k.\lambda}{\beta.cos\theta}$$

where D is the crystallite size (nm), k is the Scherrer constant which depends on the shape of the crystal (approximately 0.9 for spherical particles), λ is the wavelength of X-ray (nm), β is the full width at half maximum (FWHM) of the peak, and θ is the Bragg's angle.

A scanning electron microscope (SEM, QUANTA 250 FEG) was used to investigate the effects of doping and heat treatment temperature on the nanostructure evolution of unsupported NF membrane layers. A transmission electron microscope (TEM, JEOL JEM 2100) was used in HR-TEM imaging mode to gain more information on the heat treated (200-500°C) unsupported selective NF layer nanostructures.

CHAPTER 6

RESULTS AND DISCUSSION

6.1. Characterization of NF Membranes

Membrane characterization is important in developing abilities for the formation of defect-free membranes. The unsupported and supported NF membrane layer characterization must be conducted separately. Unsupported membranes can be produced by pouring the sol onto a smooth and dense substrate like a metallic surface on which gelation occurs by slow evaporation of the solvent. Relatively thicker films compared to the actual selective NF layers can be obtained and used for characterization purposes by this method (Burggraaf and Keizer 1991). These unsupported membranes were characterized by dilatometry, TGA, XRD, and HR-TEM analyses.

The sol species/particle size distribution control through sol-gel chemistry and aging may constitute a fundamental issue in nanostructure development and subnano NF membrane design. The sol species size distributions in 15% ZrO_2 doped (90, 120, 180 minutes of aging) and 3% Nd doped (3 days of aging) titania sols are given in Figure 6.1. Zirconia doped titania sol particle size was determined as 2.4 nm at 90^{th}, 3.6 nm in 120^{th} and 180^{th} minutes of aging. The size of the polymeric species in 3% neodymium doped titania sol was found as 3.8 nm after 3 days of aging.

Thermogravimetric behaviors of undoped/doped (1% and 3% Nd) unsupported titania membrane powders are given in Figure 6.2. The %weight losses of both neodymium doped and undoped titania unsupported membranes were between 34-36% and most of this weight loss is due to the alcohol and water removal from the structure up to 100°C. The second significant weight loss occurred in between 100-400°C which is most probably associated with the removal of nitrates and other organic matters from the powder. This deduction is supported by the increase of the %weight loss in 3% doped sample compared to the undoped sample due to the presence of nitrates. The presence of negligible weight loss in the 400-800°C range and the sample gravimetric stability occurrence at 400°C would be stated as the main result of TGA characterization.

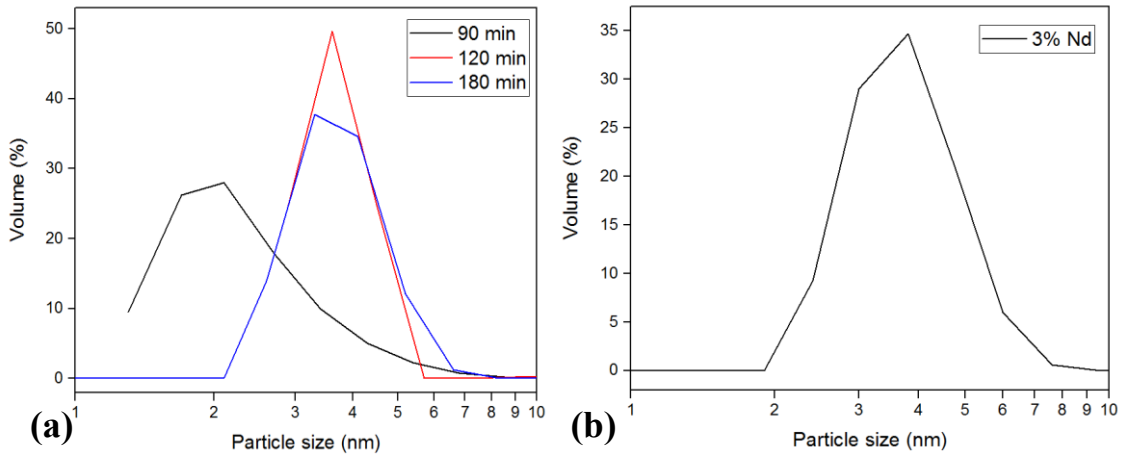

Figure 6.1. Particle size distributions of polymeric NF membrane sols (a) 15% ZrO_2 doped at 90, 120, 180 min; (b) 3% neodymium doped aged for 3 days.

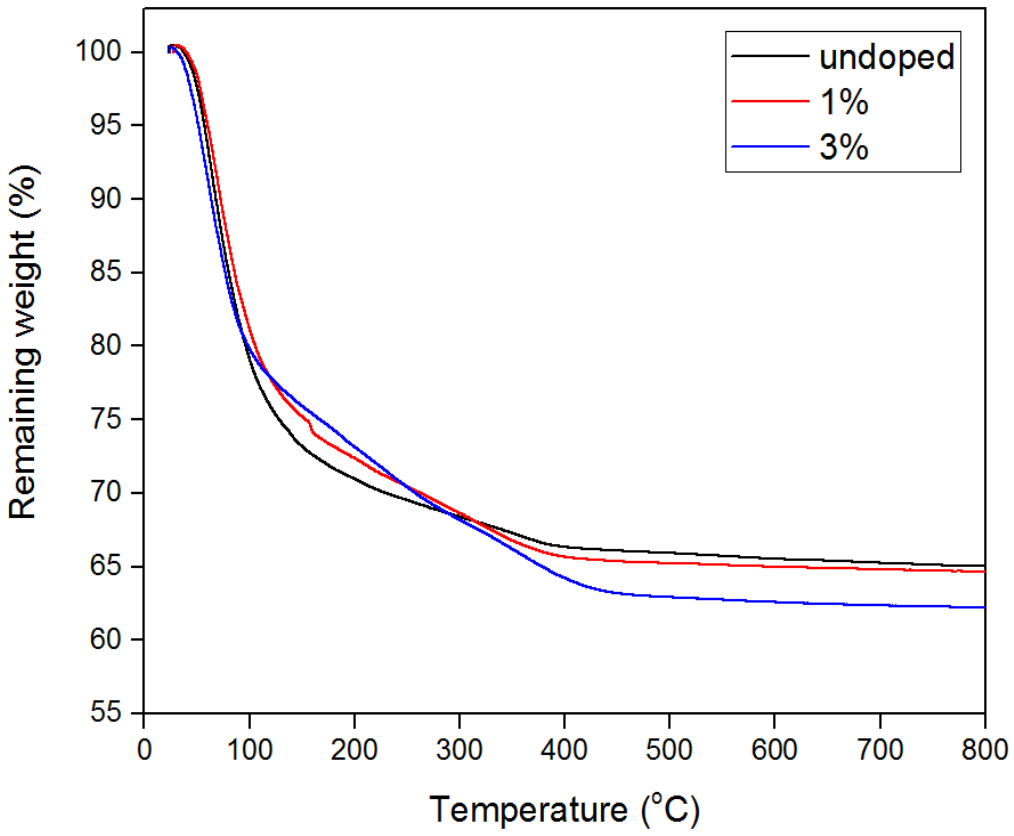

Figure 6.2. Thermogravimetric behavior of undoped and neodymium doped titania unsupported membrane powders.

Dilatometric methods were used to develop a better understanding of the neodymium/zirconium doping on phase evolution/shrinkage behavior of titania based selective NF membrane layers.

Dilatometric ΔL (μm) vs. temperature plots of neodymium doped/undoped samples are given in Figure 6.3. Pellets with similar initial sizes experience a notable decrease in ΔL values (a decrease of ΔL from about 1200 to 600 μm) with neodymium doping below 600°C which may be of great value in NF membrane preparation. The relatively sharp changes in ΔL levels observed in pure TiO_2 in the 400-600°C range was delayed to higher temperatures in doped samples. These shrinkage level variations with heat treatment temperature indicated that neodymium doping leads to critical changes in titania nanostructure evolution.

Dilatometric ΔL vs. temperature plots of titania-zirconia mixed-oxide samples are given in Figure 6.4. In membrane preparation temperature ranges ΔL values of TiO_2-ZrO_2 mixed-oxide unsupported membrane pellets were found to be significantly lower than that of pure TiO_2 and pure ZrO_2, especially in low ZrO_2 molar ratios given in Figure 6.4a. The ΔL values for 75% ZrO_2 sample was determined to be comparable to the pure ZrO_2 shrinkage levels given in Figure 6.4b. These findings show that crack-free membranes can most likely be obtained up to 25% ZrO_2 on a molar basis due to their low ΔL values. The relatively sharp changes observed in ΔL vs. Temperature plots for pure TiO_2 in the 400-600°C range was at a considerably lower levels in mixed-oxide samples.

Crack/defect formation upon the heat treatment of ceramic bodies are known to be strongly related to their shrinkage behavior. Low percentage shrinkage values may contribute to the preparation of crack-free nanofiltration membranes. Percentage shrinkage values of the bodies were calculated by taking the initial pellet dimensions as the basis and using the raw ΔL data in order to develop a better understanding of neodymium/zirconium doping effect on shrinkage behavior of unsupported TiO_2 NF membrane powders.

The dilatometric linear shrinkage vs. temperature plots of undoped TiO_2 and neodymium doped TiO_2 unsupported membrane pellets are given in Figure 6.5. It is obviously seen that neodymium doping reduces linear shrinkage values of the dry pressed ceramic bodies. The linear shrinkage values were approximately reduced by half with neodymium doping at 600°C (a decrease of percentage shrinkage from about 27 to 14 %) especially in the 1.0-4.0% doping level range in molar oxide (Nd_2O_3) basis as shown in Figure 6.5a and Figure 6.5b.

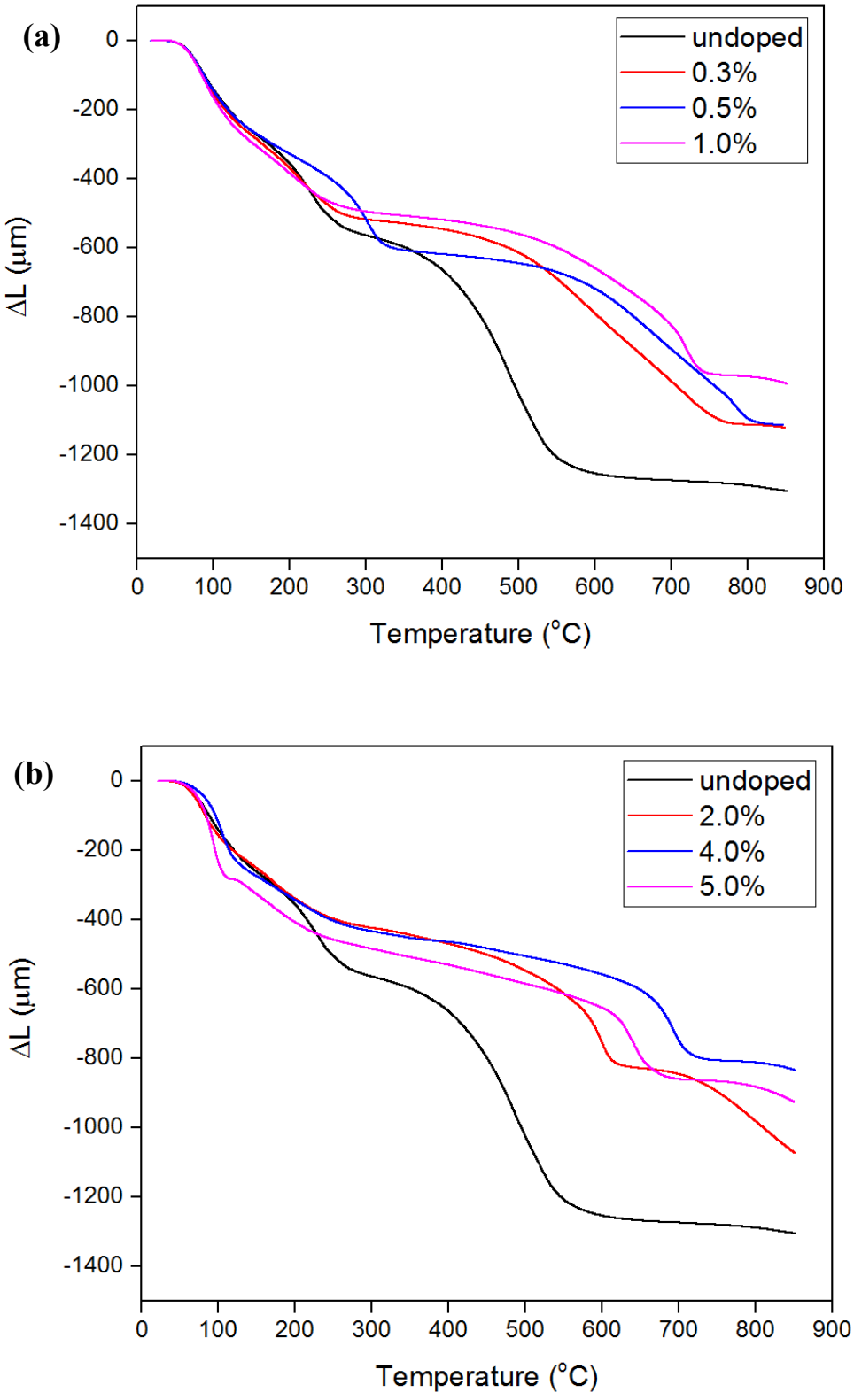

Figure 6.3. Dilatometric ΔL vs. temperature plots of undoped TiO_2 and neodymium doped (a) 0.3%, 0.5%, and 1.0% Nd; (b) 2.0%, 4.0, and 5.0% Nd TiO_2 unsupported selective NF membrane pellets.

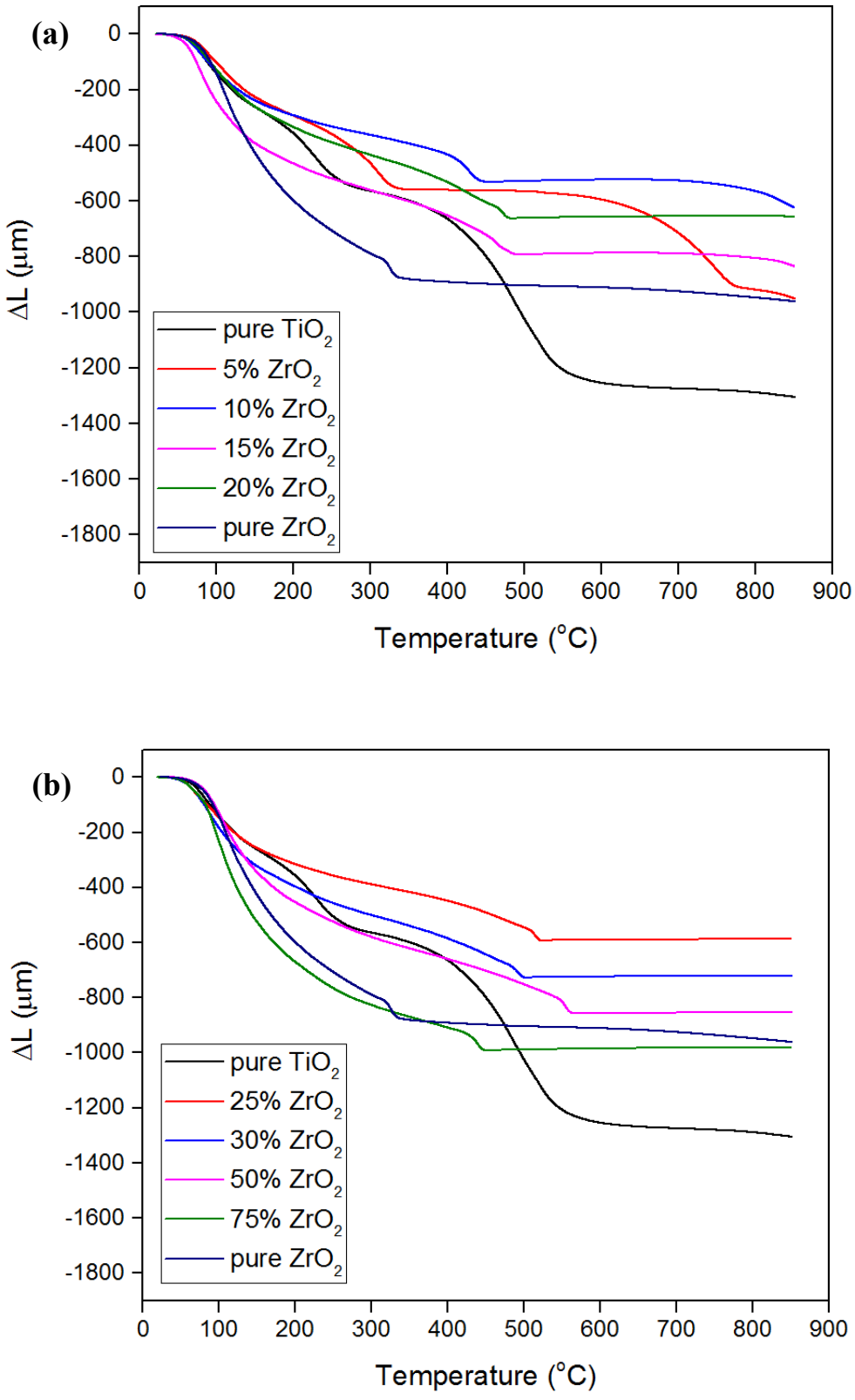

Figure 6.4. Dilatometric ΔL vs. temperature plots of pure TiO_2, pure ZrO_2, and TiO_2-ZrO_2 mixed-oxide (a) 5%, 10%, 15% and 20% ZrO_2; (b) 25%, 30%, 50%, and 75% ZrO_2 unsupported selective NF membrane pellets.

The dilatometric linear shrinkage vs. temperature plots of undoped TiO_2, ZrO_2, and TiO_2-ZrO_2 mixed-oxide unsupported selective NF membrane pellets are given in Figure 6.6. The percentage shrinkage values were approximately reduced by half at 600°C (a decrease of percentage shrinkage from about 27 to 12.5 %) which indicates similar behavior as the neodymium doping case. The most significant reductions in the percentage shrinkage values were observed at low zirconia levels (in between 5-25% ZrO_2 range in molar oxide basis) as shown in Figure 6.6a and Figure 6.6b.

Neodymium doping results in an important retardation in the temperature ranges (observed as peaks) at which accelerated densification/phase evolution occur as observed in the dilatometric shrinkage rate plots in Figure 6.7. The first peak observed at around 100°C is related to the densification due to packing/reorganization of polymeric species during the ethanol/water removal from the unsupported membrane pellet. This packing leads to about 5% volumetric shrinkage in the body. The second series of peaks observed between 200-300°C may also be about the ongoing amorphous to crystalline transformation. Neodymium doping at low levels prevented the anatase to rutile phase transformation. The main peak observed in the 375-550°C range for undoped TiO_2 may be associated with anatase crystallite growth/sintering/densification. This temperature range coincides with the heat treatment temperatures of NF membranes where the formation of cracks and pinholes may become possible. This main peak was shifted with various levels of neodymium doping by about 200°C.

Dilatometric shrinkage rate plots of pure TiO_2, ZrO_2, and TiO_2-ZrO_2 mixed-oxide unsupported selective membrane pellets are given in Figures 6.8 and 6.9. Pure zirconia has a very narrow peak in the 315-335°C range. A significantly different behavior was exhibited for TiO_2-ZrO_2 mixed-oxide membranes with 5% ZrO_2 and 10% ZrO_2 compared to both pure TiO_2 and pure ZrO_2 as seen in Figure 6.8a. The peaks of 5% ZrO_2 and 10% ZrO_2 containing samples were observed between 230-330°C and 400-450°C, respectively. TiO_2-ZrO_2 mixed-oxide membranes with 15% ZrO_2 and 20% ZrO_2, these temperature ranges became narrower and shifted (Figure 6.8b). This trend continues in 25% ZrO_2 and 30% ZrO_2 mixed-oxide samples (Figure 6.9a) and the peak range shifts to 540-565°C in the equimolar TiO_2-ZrO_2 unsupported membrane (Figure 6.9b). This range was observed at a lower temperature (420-445°C) in 75% ZrO_2 sample which was closer to the peak range of pure ZrO_2.

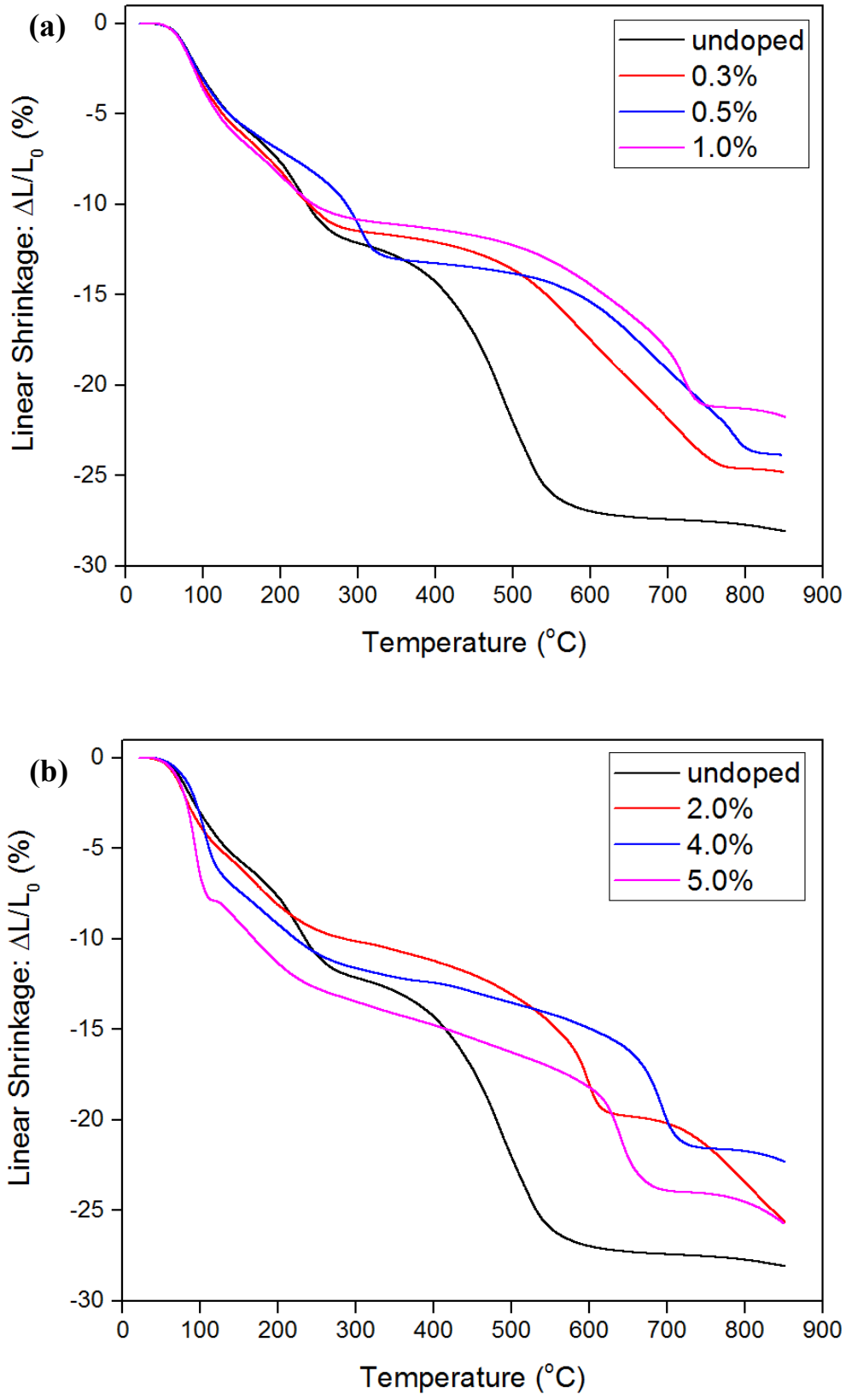

Figure 6.5. Dilatometric linear shrinkage vs. temperature plots of undoped TiO_2 and neodymium doped (a) 0.3%, 0.5%, and 1.0% Nd; (b) 2.0%, 4.0, and 5.0% Nd TiO_2 unsupported selective NF membrane pellets.

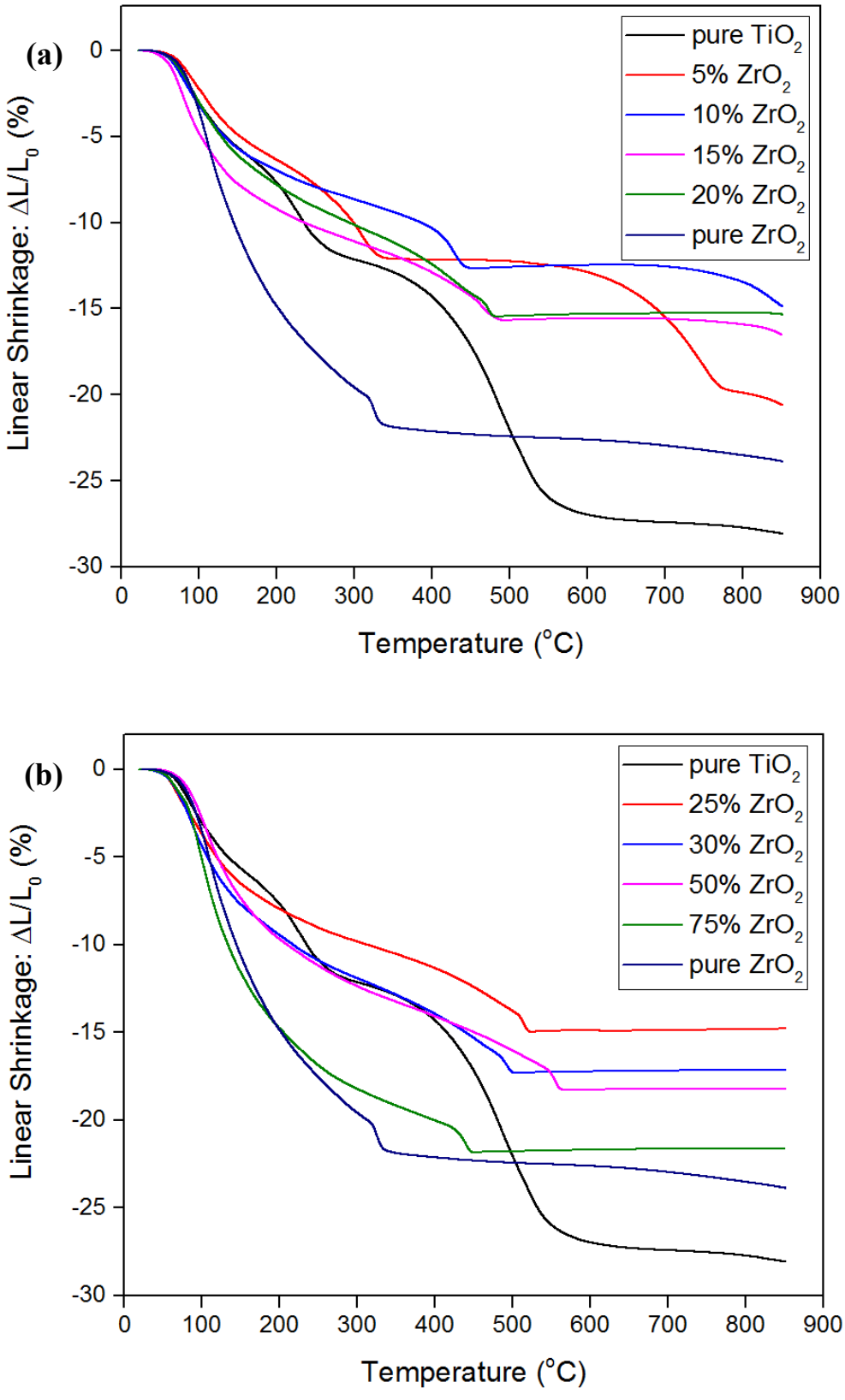

Figure 6.6. Dilatometric linear shrinkage vs. temperature plots of pure TiO_2, pure ZrO_2, and TiO_2-ZrO_2 mixed-oxide (a) 5%, 10%, 15% and 20% ZrO_2; (b) 25%, 30%, 50%, and 75% ZrO_2 unsupported selective NF membrane pellets.

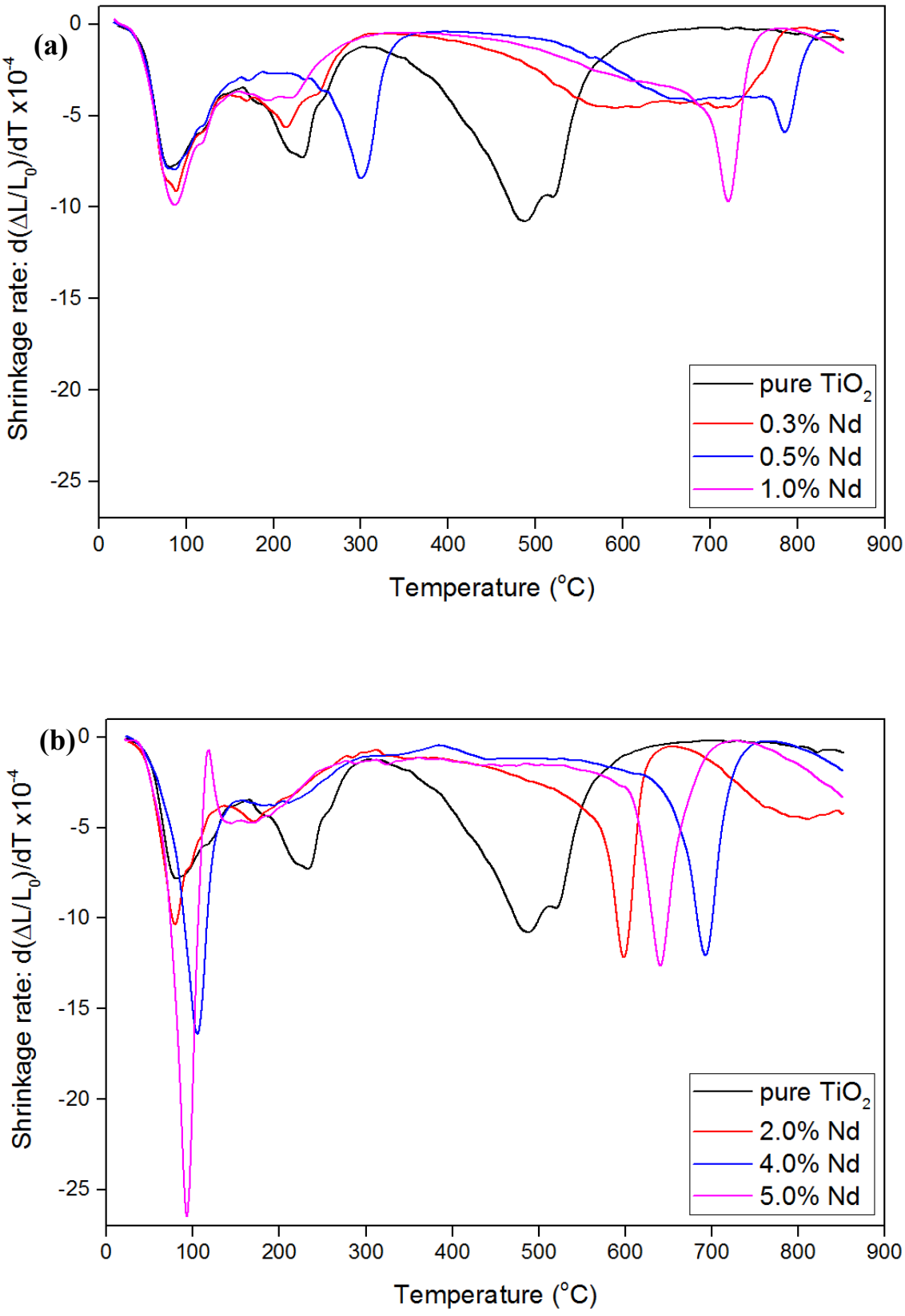

Figure 6.7. Dilatometric shrinkage rate plots of undoped TiO_2 and neodymium doped (a) 0.3%, 0.5%, and 1.0% Nd; (b) 2.0%, 4.0, and 5.0% Nd TiO_2 unsupported selective NF membrane pellets.

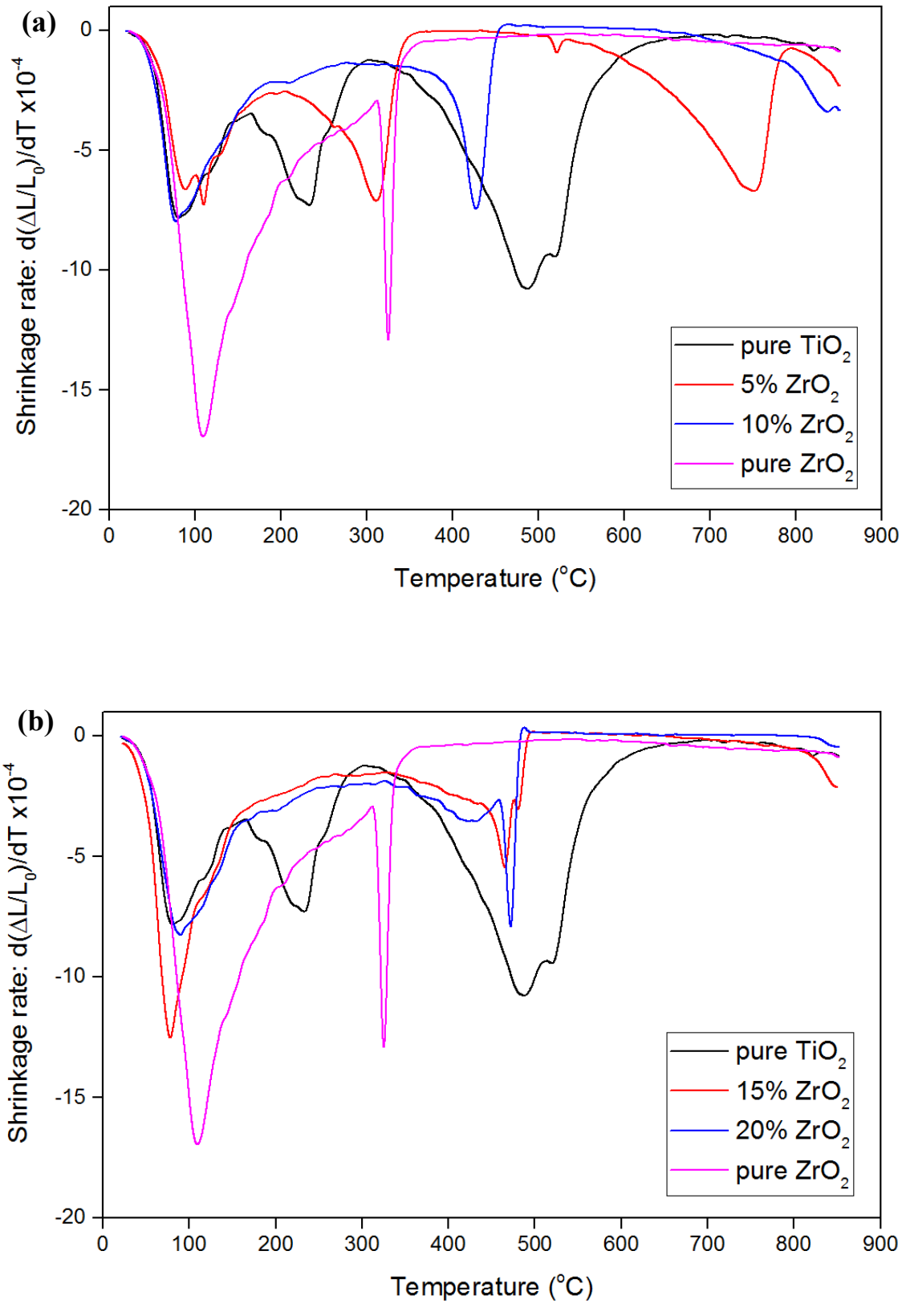

Figure 6.8. Dilatometric shrinkage rate plots of pure TiO_2, pure ZrO_2, and TiO_2-ZrO_2 mixed-oxide (a) 5%, 10% ZrO_2; (b) 15%, 20% ZrO_2 unsupported selective NF membrane pellets.

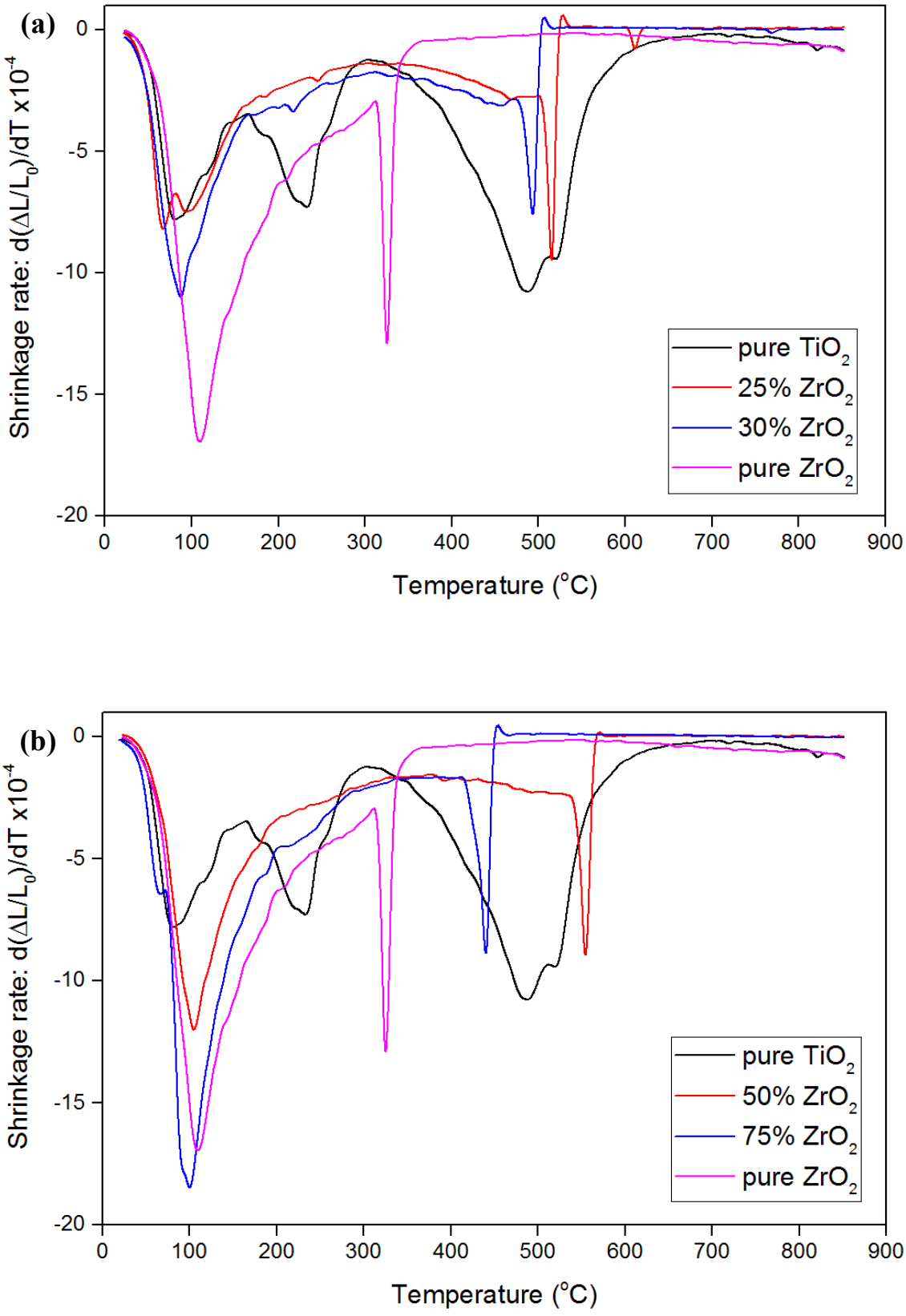

Figure 6.9. Dilatometric shrinkage rate plots of pure TiO_2, pure ZrO_2, and TiO_2-ZrO_2 mixed-oxide (a) 25%, 30% ZrO_2; (b) 50%, 75% ZrO_2 unsupported selective NF membrane pellets.

The dilatometric density vs. temperature plots constructed by assuming equal shrinkage in both dimensions are given in Figures 6.10 and 6.11. The densities of neodymium doped unsupported membranes were determined to be in between 1.80-1.95 g/cm^3 at neodymium doping levels lower than 1% as shown in Figure 6.10a. The densities were also determined to be in between 2.15-2.45 g/cm^3 at neodymium doping levels in between 2-5% as shown in Figure 6.10b. The densities of TiO_2-ZrO_2 mixed-oxide unsupported membranes at 600°C were found in between 1.75-2.15 g/cm^3 for lower zirconia percentages (5-20%) and in between 2.15-2.80 g/cm^3 for higher zirconia percentages (25-75%) as shown in Figures 6.11a and 6.11b. All density values were significantly lower than the density of undoped TiO_2 and ZrO_2 which indicates that both neodymium doping and zirconium mixing hinders the densification of selective titania NF membrane layers.

A detailed XRD analysis was performed in order to support dilatometric phase evolution findings on phase transformations. Thin unsupported membrane layers which were prepared by drying in a high surface area metal tray overnight at room temperature mimicking selective NF membrane layer formation were heat treated in the 200-500°C range. No dwell time was used at maximum temperature in order to make a proper comparison between dilatometric curves and XRD patterns. The XRD patterns of neodymium doped TiO_2 powders heat treated at different temperatures are given in Figure 6.12. The peak intensities were reduced and became broader with neodymium doping. This broadening brings about a decrease in crystallite size of the anatase phase. These findings are consistent with the dilatometric shrinkage rate curves seen in Figure 6.7 due to the retardation of temperature ranges with neodymium doping. All of the observed peaks in Figure 6.12 belong to the anatase phase of titania. Anatase crystallite sizes can be calculated using the main peak at $2\theta=25.3°$ however the calculated crystallite sizes may include some errors because of the very small crystallite sizes of particularly in higher neodymium doping levels. The crystallite sizes of titania anatase phase calculated by using Scherrer's equation for neodymium doped titania samples are given in Table 6.1. Anatase crystallite sizes were significantly increased with heat treatment temperature but very small crystallite sizes compared to pure titania were obtained at low neodymium doping levels. XRD patterns of pure TiO_2, pure ZrO_2, and TiO_2-ZrO_2 mixed-oxide unsupported membrane powders are given in Figure 6.13. The peak intensities of the anatase phase increased and the peaks became sharper with heat treatment temperature

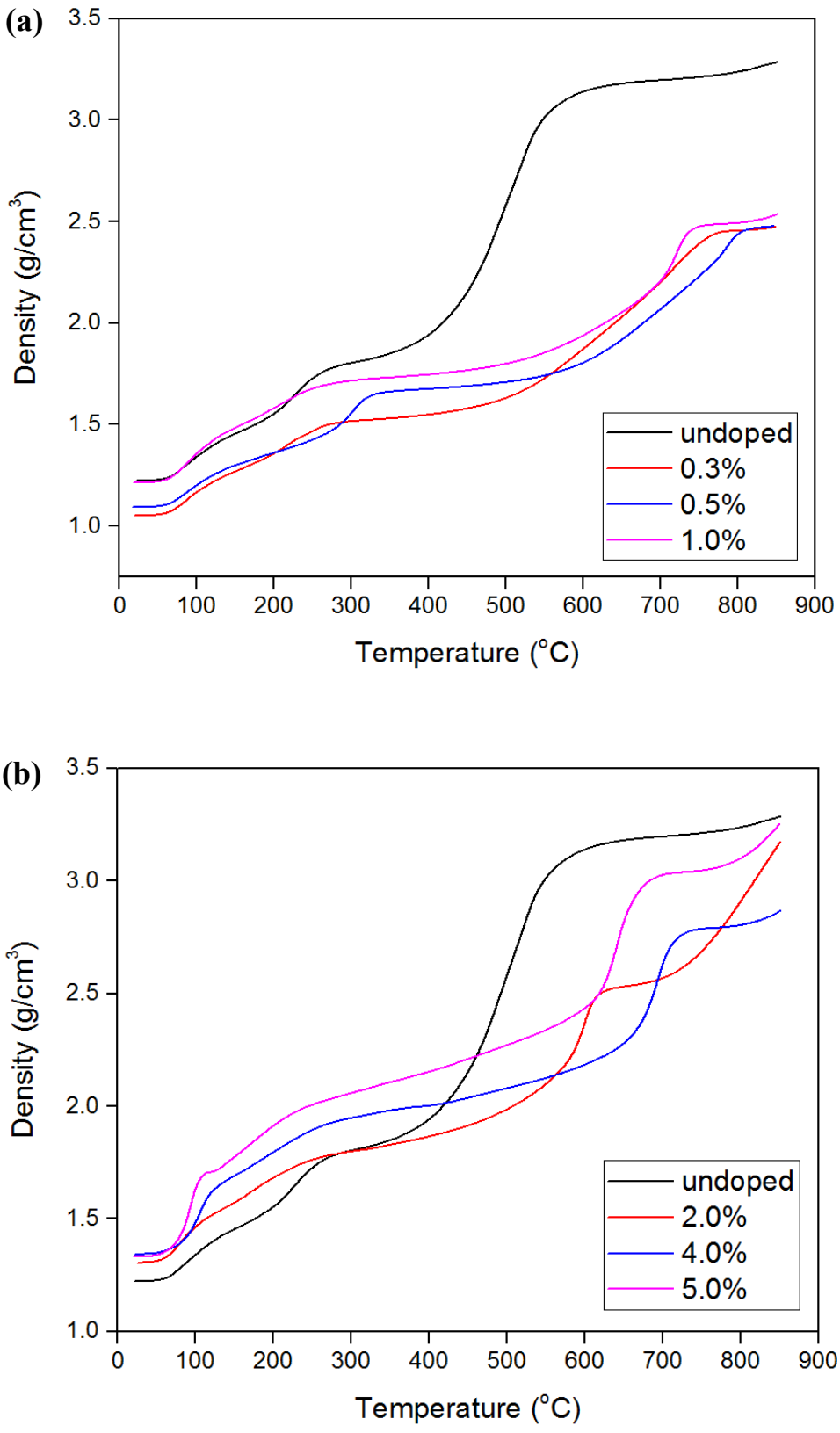

Figure 6.10. Dilatometric temperature vs. density plots of undoped TiO_2 and neodymium doped (a) 0.3%, 0.5%, and 1.0% Nd; (b) 2.0%, 4.0, and 5.0% Nd TiO_2 unsupported selective NF membrane pellets.

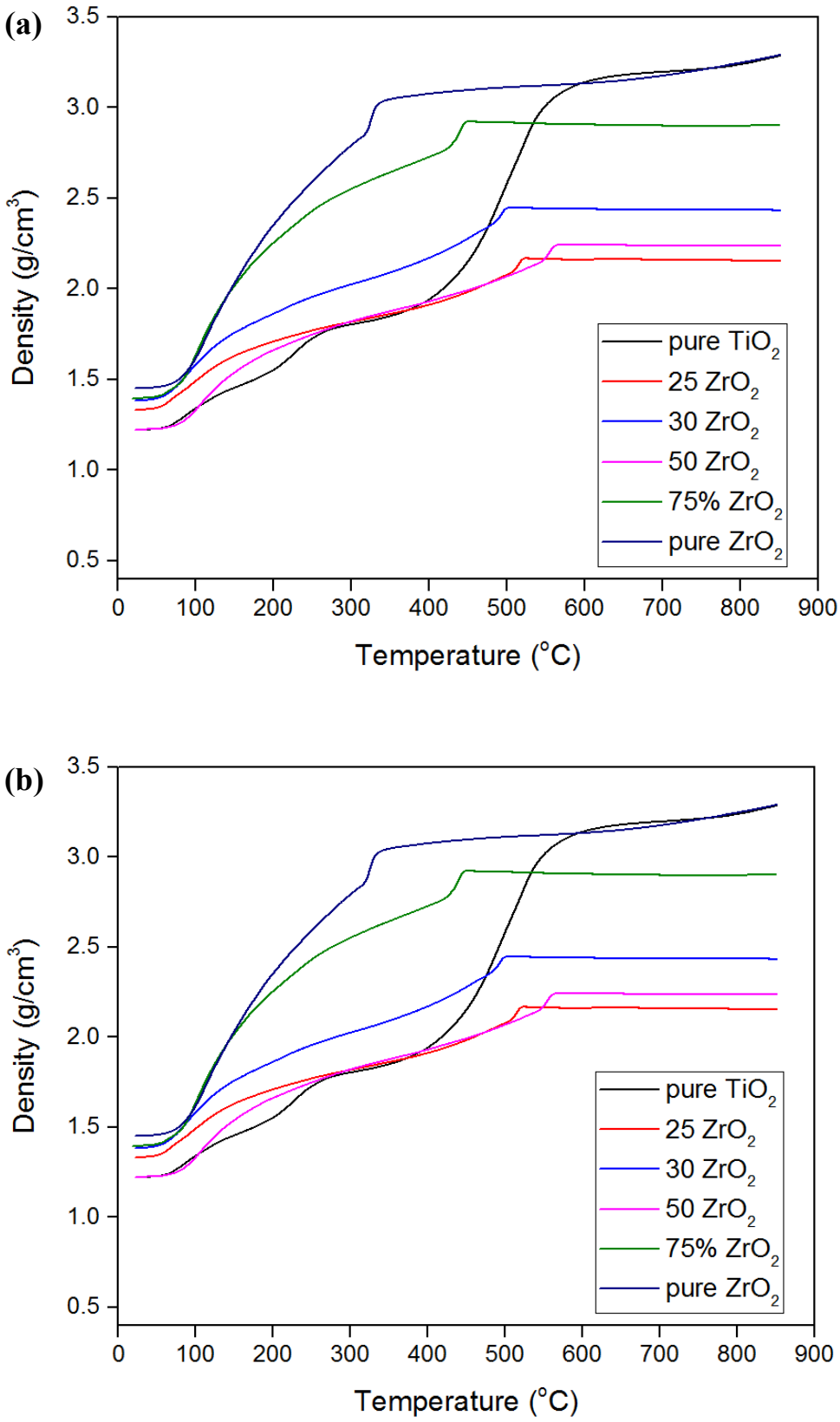

Figure 6.11. Dilatometric temperature vs. density plots of pure TiO_2, pure ZrO_2, and TiO_2-ZrO_2 mixed-oxide (a) 5%, 10%, 15% and 20% ZrO_2; (b) 25%, 30%, 50%, and 75% ZrO_2 unsupported selective NF membrane pellets.

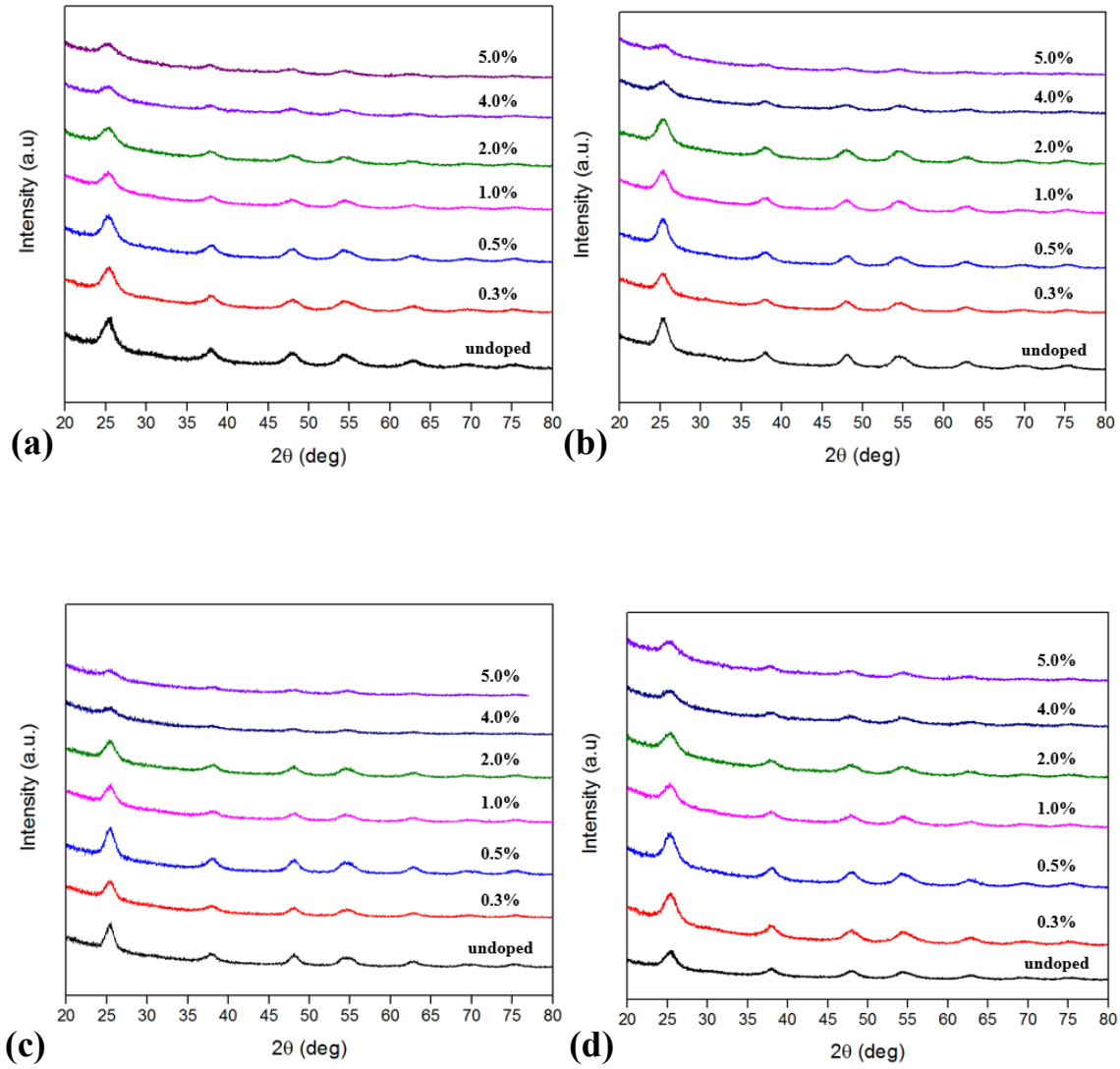

Figure 6.12. XRD patterns of neodymium doped TiO_2 unsupported NF membrane powders heat treated at (a) 250°C, (b) 350°C, (c) 400°C, and (d) 500°C.

Table 6.1. Anatase crystallite sizes of neodymium doped/undoped TiO_2 unsupported NF membrane powders at different heat treatment temperatures.

	Pure TiO_2	0.3% Nd	0.5% Nd	1.0% Nd	2.0% Nd	4.0% Nd	5.0% Nd
250°C	5.7 nm	4.2 nm	4.5 nm	3.4 nm	3.6 nm	<3.0 nm	<3.0 nm
350°C	6.0 nm	5.5 nm	5.7 nm	5.1 nm	4.4 nm	<3.0 nm	<3.0 nm
400°C	7.0 nm	6.1 nm	5.5 nm	3.7 nm	4.0 nm	<3.0 nm	<3.0 nm
500°C	8.9 nm	6.9 nm	6.5 nm	6.2 nm	5.2 nm	3.2 nm	3.7 nm

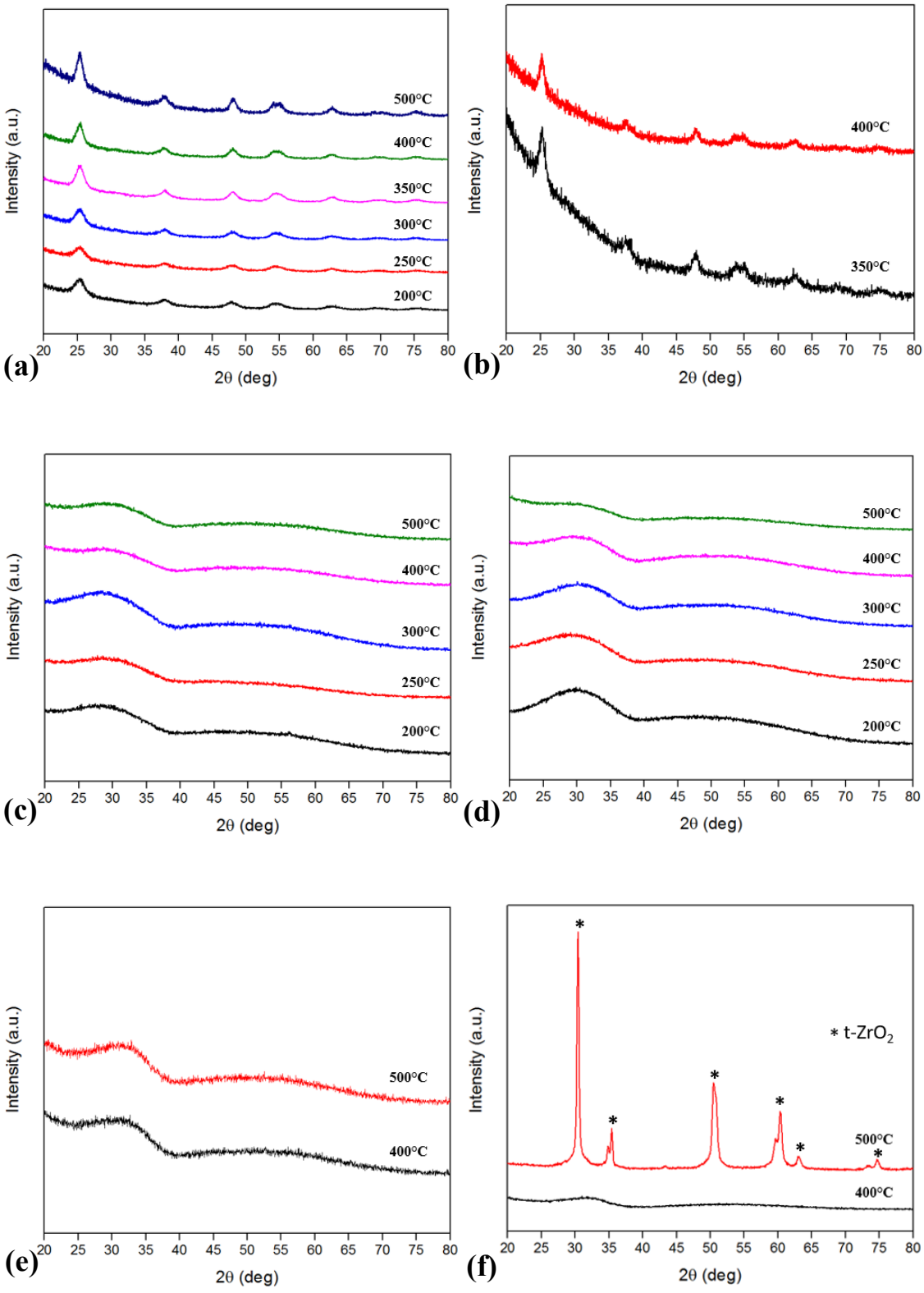

Figure 6.13. XRD patterns of TiO_2-ZrO_2 mixed-oxide unsupported NF membrane powders containing (a) pure TiO_2, (b) 10% ZrO_2, (c) 20% ZrO_2, (d) 30% ZrO_2, (e) 50% ZrO_2, and (f) pure ZrO_2 at different heat treatment temperatures.

for pure titania. The anatase peaks are still observed at 350°C for 10% ZrO_2 mixed TiO_2 membrane powder (Figure 6.13b) whereas the powder was amorphous for 20% ZrO_2 mixed TiO_2 even at 500°C as seen in Figure 6.13c. This indicates the important effect of zirconium mixing in titania membranes which may contribute to the nanostructure evolution in NF layer formation through micropore size control in the amorphous state. The amorphous nature of membrane powders continued to be observed with the increased ZrO_2 mixing levels as can be observed in Figures 6.13c, 6.13d, and 6.13e.

SEM characterization was conducted in order to investigate the effects of doping and heat treatment temperature on the nanostructure evolution of unsupported NF membrane layers. The SEM image of 4% Nd doped TiO_2 unsupported NF membrane powders heat treated at 400°C is given in Figure 6.14. The SEM image of 20% ZrO_2 TiO_2-ZrO_2 mixed-oxide unsupported NF membrane powders heat treated at 400°C is given in Figure 6.15. The resolution/magnifications of these SEM images were not high enough for obtaining valuable information on the nanostructure of these NF candidate powders. The HR-TEM characterization was performed for the investigation of the nanostructure and the detection of present phases in the unsupported membrane powders. The Fast Fourier Transform (FFT) of the HR-TEM images were obtained by using ImageJ 1.50b software. Interplanar spacing (d-spacing) values are given below the FFT of related HR-TEM images.

HR-TEM image of 4% Nd doped TiO_2 unsupported membrane powders without heat treatment with its corresponding FFT image is given in Figure 6.16. The highlighted crystallite was determined to be 3.7 nm in size. FFT image shows that the d-spacing is 0.34 nm which corresponds to the (101) crystallographic plane of anatase TiO_2. HR-TEM image of 4% Nd doped TiO_2 unsupported membrane powders heat treated at 200°C with its corresponding FFT image is shown in Figure 6.17. The highlighted crystallite was found to be 5.4 nm in size. FFT image shows that the d-spacing is 0.34 nm which corresponds to (101) crystallographic plane of anatase TiO_2. HR-TEM image of 4% Nd doped TiO_2 unsupported membrane powders heat treated at 400°C with its corresponding FFT image is shown in Figure 6.18. The highlighted crystallite was determined to be 6.2 nm in size. FFT image shows that the d-spacing is 0.34 nm which corresponds to (101) crystallographic plane of anatase TiO_2. Anatase was the only phase detected in HR-TEM images of these unsupported membrane powders.

HR-TEM image of TiO_2-ZrO_2 unsupported membrane powders containing 20% ZrO_2 heat treated at 200°C is given in Figure 6.19. This powder was determined to be

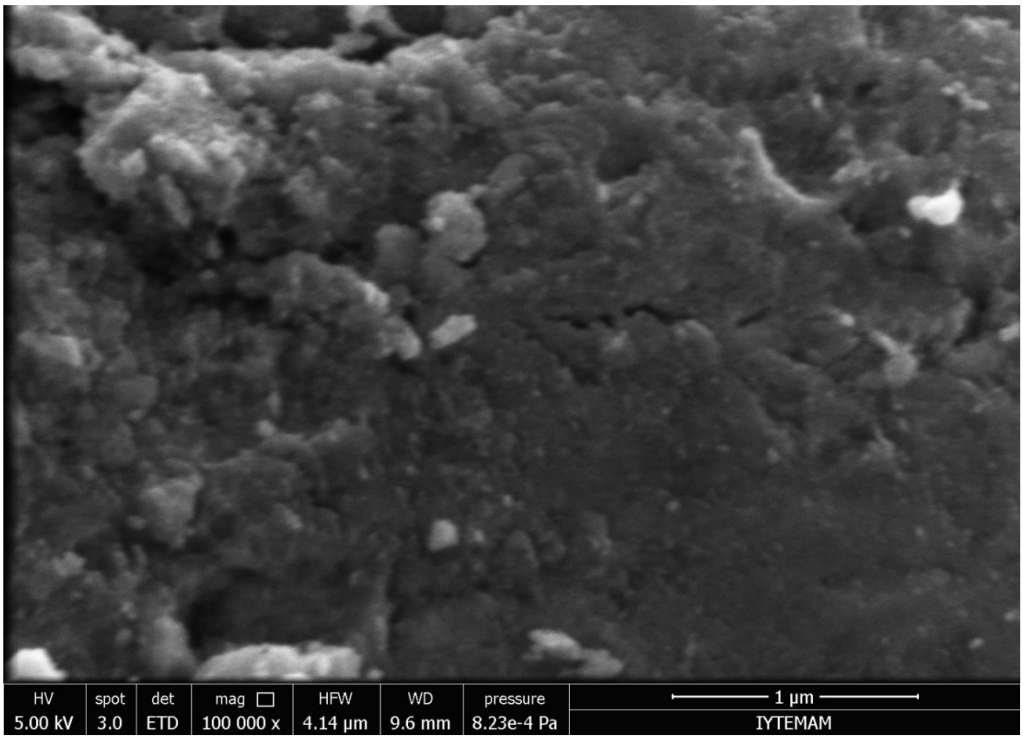

Figure 6.14. SEM image of 4% Nd doped TiO_2 unsupported NF membrane powders heat treated at 400°C.

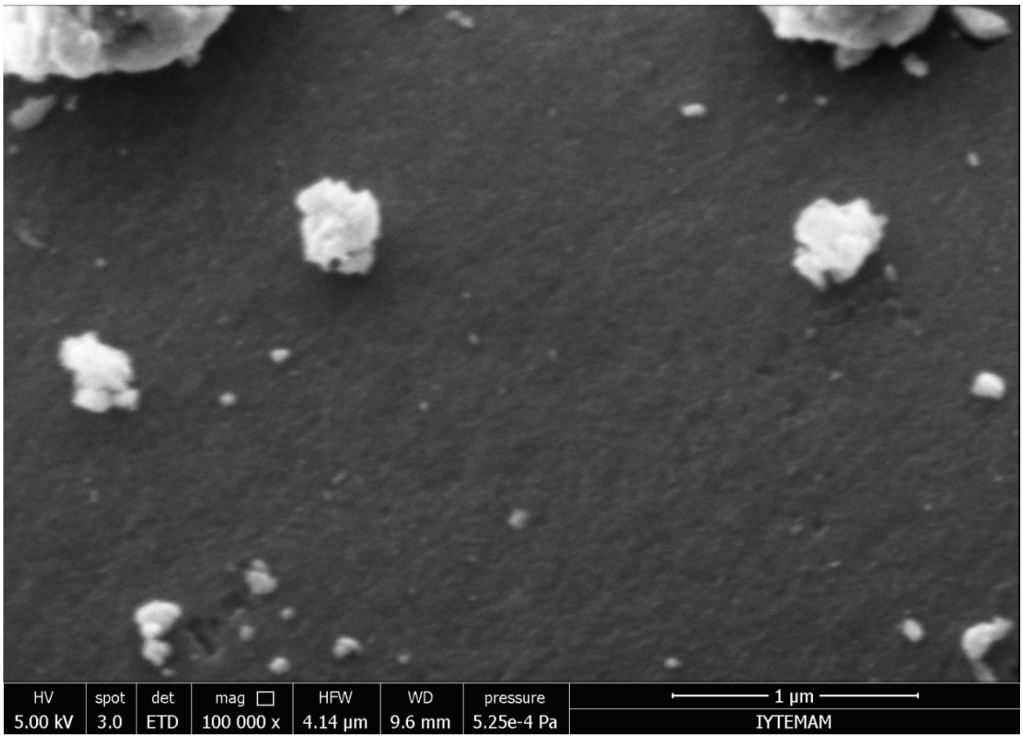

Figure 6.15. SEM image of 20% ZrO_2 TiO_2-ZrO_2 mixed-oxide unsupported NF membrane powders heat treated at 500°C.

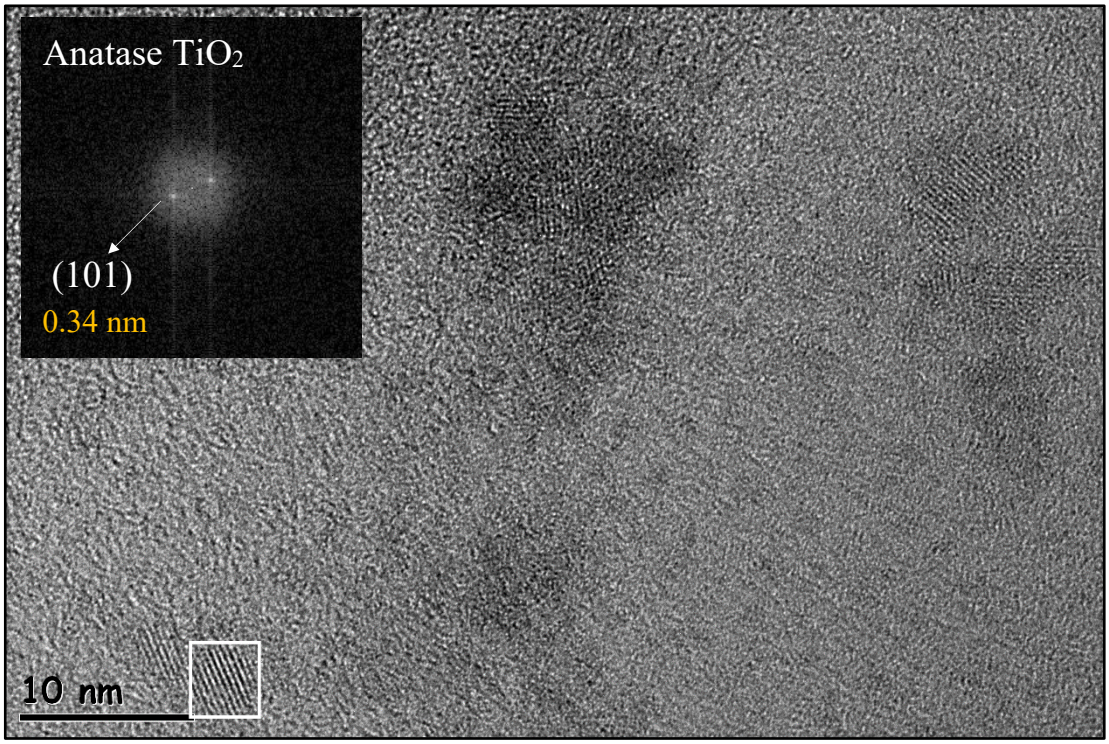

Figure 6.16. HR-TEM image of 4% Nd doped TiO_2 unsupported NF membrane powders without heat treatment.

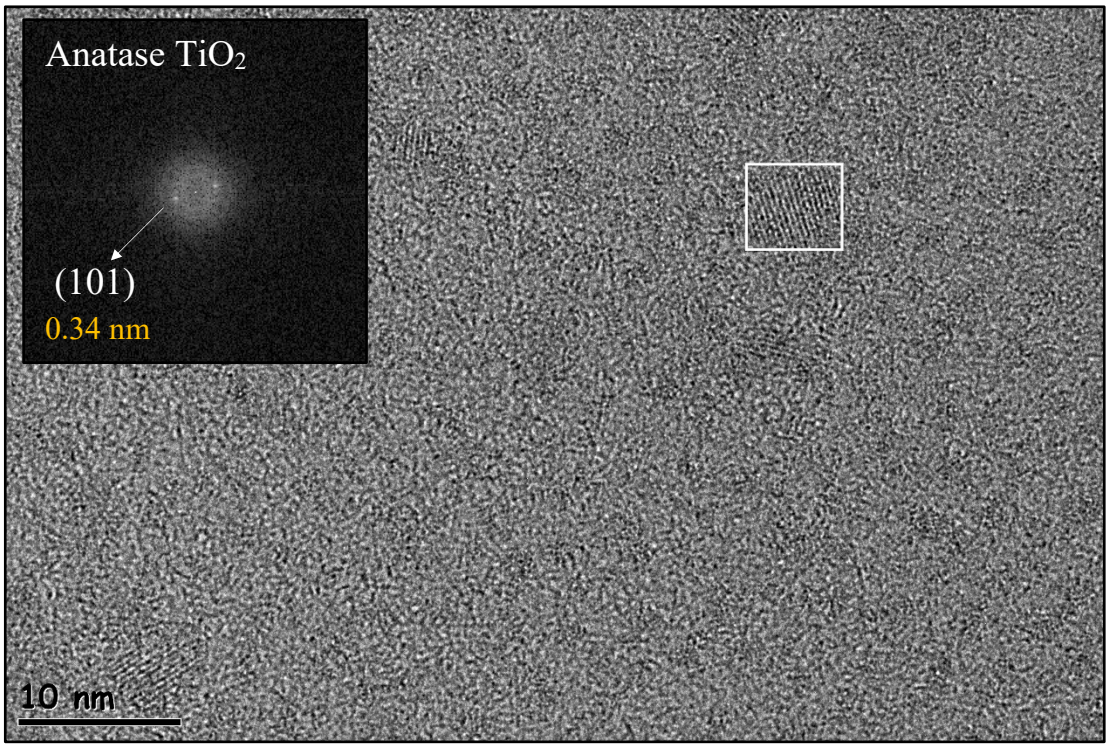

Figure 6.17. HR-TEM image of 4% Nd doped TiO_2 unsupported NF membrane powders heat treated at 200°C.

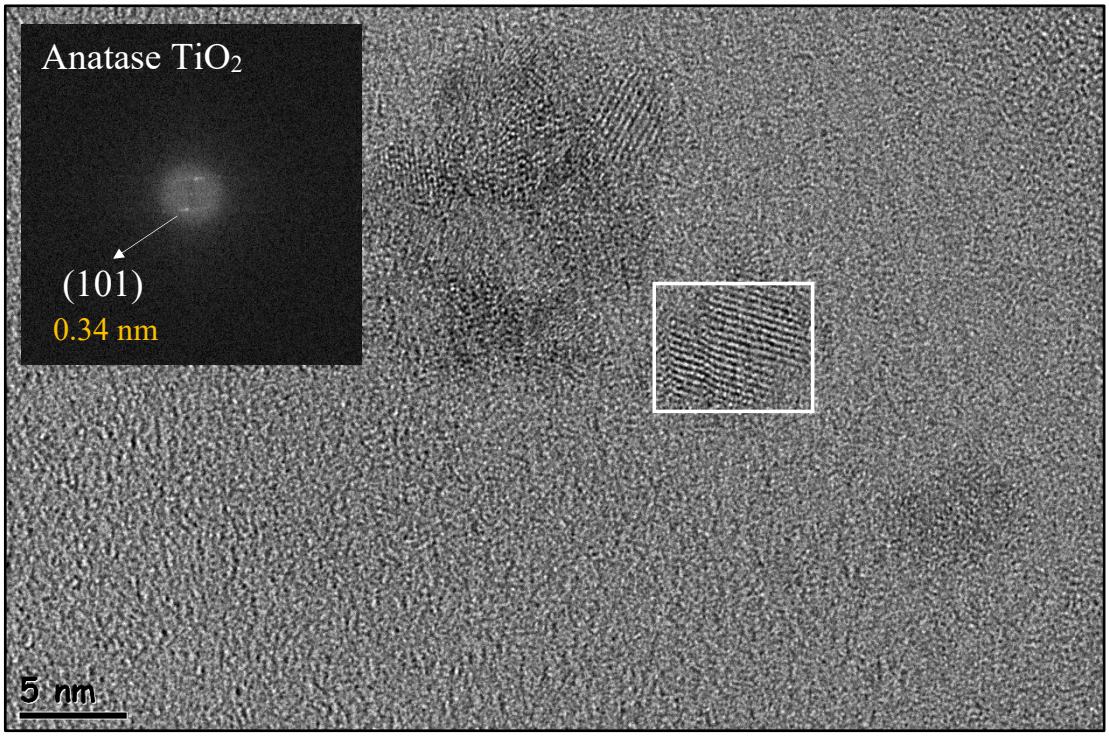

Figure 6.18. HR-TEM image of 4% Nd doped TiO_2 unsupported NF membrane powders heat treated at 400°C.

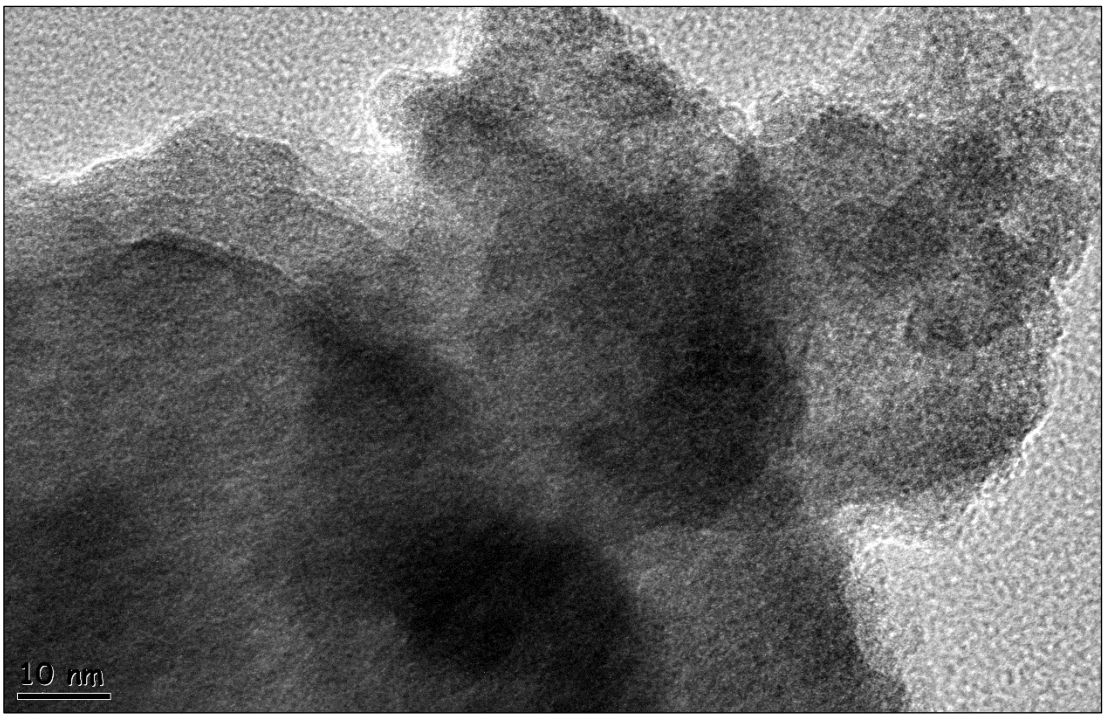

Figure 6.19. HR-TEM image of TiO_2-ZrO_2 unsupported NF membrane powders containing 20% ZrO_2 heat treated at 200°C.

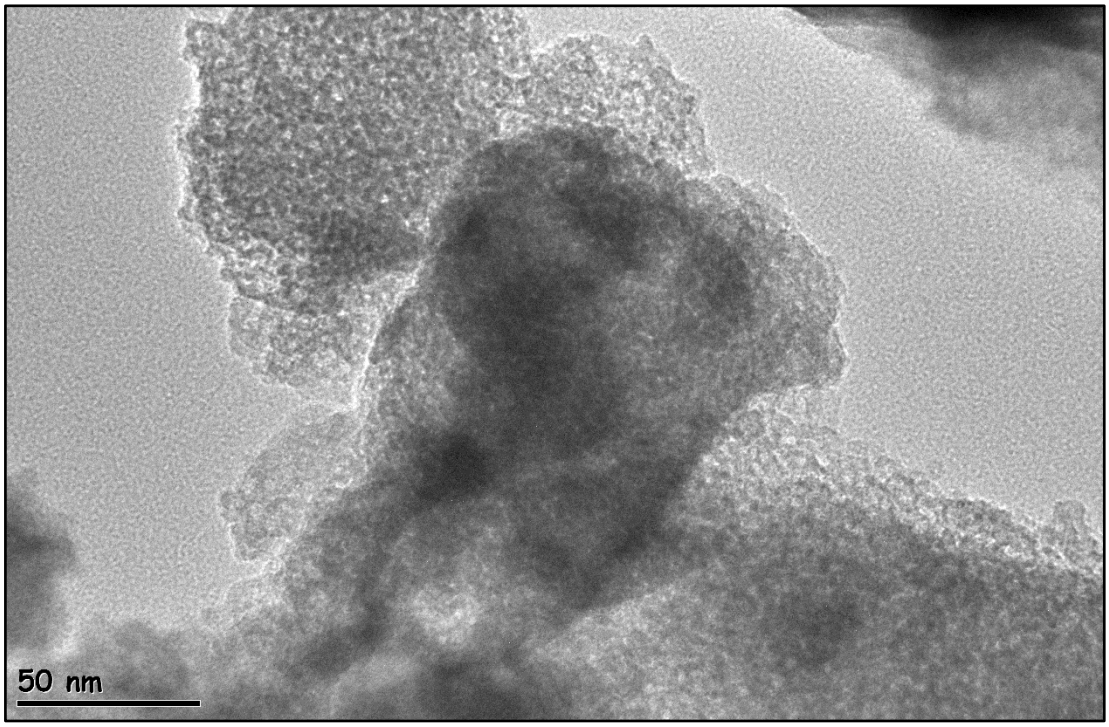

Figure 6.20. HR-TEM image of TiO_2-ZrO_2 unsupported NF membrane powders containing 20% ZrO_2 heat treated at 500°C.

amorphous which is consistent with the XRD diffractogram illustrated in Figure 6.13c. HR-TEM image of the same powder heat treated at 500°C is given in Figure 6.20. The structure was observed to be amorphous which is also consistent with the XRD results given in Figure 6.13c. The amorphous structure seen in the 20% ZrO_2 mixed-oxide unsupported membrane up to 500°C will undoubtedly contribute to the selective NF membrane layer preparation.

6.2. Recommendations on MWCO Determination for Future Work

Molecular weight cut-off determination and filtration experiments should be conducted in the cross-flow filtration set up shown in Figure 6.21. This filtration set up consists of a membrane module, a pump, a flow controller, two pressure gauges, and two needle valves. Cross-flow velocity can be adjusted by means of the pump, and pressure can be controlled by means of the needle valves.

Aqueous PEG solutions will be used in separation capacity determination of tubular ceramic membranes. This will be conducted by the detection of refractive index

Figure 6.21. The filtration set-up used in MWCO and flux determinations.

Table 6.2. Viscosity radii of polyethylene glycols.

PEG molecular weight $M_{r,PEG}$ (Da)	PEG viscosity radii $R_{h,PEG}$ (nm)
20000	4.9
10000	3.3
2000	1.3
1000	0.9
400	0.5

variations of samples collected from permeate and retentate streams with time. Fee and Van Alstine (2004) proposed following power-law relationship to estimate viscosity radii of PEG molecules, $R_{h,PEG}$ (Å), with different molecular weights, $M_{r,PEG}$ (Da).

$$R_{h,PEG} = 0.1912 M_{r,PEG}^{0.559}$$

Viscosity radii of all PEG molecules used in MWCO determinations are calculated by using this equation and listed in Table 6.1.

CHAPTER 7

CONCLUSIONS

The removal of organic/ionic species from solutions by using membrane based NF processes would have a great potential impact on energy efficient separation problems and environmental problems of today and the future. These are known as subnano membranes and ceramic nanostructures are preferred due to their superior chemical/thermal/mechanical properties compared to their polymeric counterparts. The abilities developed on the nanodesign of these ceramic nanostructures may have a critical role on human living standards. The effect of neodymium doping and zirconium mixing on nanostructural evolution of the selective titania NF membrane layers for the rejection of subnano sized organic compounds were investigated by using a number of characterization methods in this work.

The average particle size of the polymeric NF sol species/particles synthesized by sol-based methods were determined to be in the 2-4 nm size range. The sol species/particle size distribution control through sol-gel chemistry and aging may constitute a fundamental issue in nanostructure development and subnano NF membrane design. TGA results indicated that the %weight losses of both neodymium doped and undoped titania unsupported membranes were approximately 35% and most of this weight loss is associated with the solvent removal from the body up to 100°C. Another significant weight loss was observed in the 100-400°C range which is most probably associated with the removal of nitrates and other organic matters from the body and sample weights became stable at 400°C.

Dilatometric characterization was used as a capable technique for the development of a better understanding on the dopant based differences in nanophase evolution/densification behavior of the membranes. Low doping levels of rare earth elements may contribute to the nanostructure tuning of ceramic NF layers. The oxide doped NF layers experience lower levels of volumetric shrinkage of the body, retardations in phase structure evolution and decrease in cystallite size while they gain thermal stability which may contribute to obtaining crack-free membrane layers. Neodymium doping (1-4%) and zirconia mixing (10-25%) in titania led to low shrinkage values and

retardation of densification behavior of titania. Amorphous structure observed in titania rich TiO_2-ZrO_2 mixed-oxide membranes may significantly contribute to the control/design of the micropore structure during the preparation of nanofiltration membrane selective layers. Both XRD diffractograms and HR-TEM images indicated that the crystallite sizes increase at higher heat treatment temperatures.

The use of dilatometric characterization on the development of a better undersanding of the nanostructure evolution/phase transformations was found to be valuable which was also supported by the TEM generated data. ZrO_2 mixed and Nd doped defect/crack free NF membranes by using the findings of this work should be prepared in the near future. The MWCOs of these membranes should be determined by using PEG solutions.

REFERENCES

Aust, U., Benfer, S., Dietze, M., Rost, A. and Tomandl, G., 2006. "Development of microporous ceramic membranes in the system TiO2/ZrO2." *Journal of Membrane Science* 281:463-471. http://dx.doi.org/10.1016/j.memsci.2006.04.016.

Benfer, S., Popp, U., Richter, H., Siewert, C. and Tomandl, G., 2001. "Development and characterization of ceramic nanofiltration membranes." *Separation and Purification Technology* 22–23:231-237. http://dx.doi.org/10.1016/S1383-5866(00)00133-7.

Bonekamp, B. C., 1996. Preparation of asymmetric ceramic membrane supports by dip-coating. In A. J. Burggraaf and L. Cot (Eds.) *Fundamentals of inorganic membrane science and technology* 227-258. https://doi.org/10.1016/S0927-5193(96)80009-X.

Brinker, C. J. and Scherer, G. W., 1990. *Sol-gel Science: The Physics and Chemistry of Sol-gel Processing*. Academic Press, Inc.

Burggraaf, A. J., 1996. Important Characteristics of Inorganic Membranes. In A. J. Burggraaf and L. Cot (Eds.) *Fundamentals of inorganic membrane science and technology* 21-34. http://dx.doi.org/10.1016/S0927-5193(96)80001-5.

Burggraaf, A. J. and Keizer, K., 1991. Synthesis of Inorganic Membranes. In R. R. Bhave (Eds.) *Inorganic Membranes Synthesis, Characteristics and Applications*

Cai, Y., Wang, Y., Chen, X., Qiu, M. and Fan, Y., 2015. "Modified colloidal sol–gel process for fabrication of titania nanofiltration membranes with organic additives." *Journal of Membrane Science* 476:432-441. http://dx.doi.org/10.1016/j.memsci.2014.11.034.

Chen, P. L., Ma, X., Zhong, Z. X., Zhang, F., Xing, W. H. and Fan, Y. Q., 2017. "Performance of ceramic nanofiltration membrane for desalination of dye solutions containing NaCl and Na2SO4." *Desalination* 404:102-111. 10.1016/j.desal.2016.11.014.

Farsi, A., Malvache, C., De Bartolis, O., Magnacca, G., Kristensen, P. K., Christensen, M. L. and Boffa, V., 2017. "Design and fabrication of silica-based nanofiltration membranes for water desalination and detoxification." *Microporous and Mesoporous Materials* 237:117-126. http://dx.doi.org/10.1016/j.micromeso.2016.09.022.

Fee, C. J. and Van Alstine, J. M., 2004. "Prediction of the Viscosity Radius and the Size Exclusion Chromatography Behavior of PEGylated Proteins." *Bioconjugate Chemistry* 15:1304-1313. 10.1021/bc049843w.

Gillot, J., 1991. The Developing Use of Inorganic Membranes: A Historical Perspective. In R. R. Bhave (Eds.) *Inorganic Membranes Synthesis, Characteristics and Applications*

Guizard, C., 1996. Sol-gel chemistry and its application to porous membrane processing. In A. J. Burggraaf and L. Cot (Eds.) *Fundamentals of inorganic membrane science and technology* 227-258. https://doi.org/10.1016/S0927-5193(96)80010-6.

Hsieh, H. P., 1996. Historical Development and Commercialization of Inorganic Membranes. In H. P. Hsieh (Eds.) *Inorganic Membranes for Separation and Reaction* 15-22. http://dx.doi.org/10.1016/S0927-5193(96)80021-0.

Jye, L. W. and Ismail, A. F., 2016. *Nanofiltration Membranes: Synthesis, Characterization and Applications*. CRC Press doi:10.1201/9781315181479-2
10.1201/9781315181479-2.

Kuzniatsova, T., Mottern, M. L., Shqau, K., Yu, D. and Verweij, H., 2008. "Micro-structural optimization of supported γ-alumina membranes." *Journal of Membrane Science* 316:80-88. http://dx.doi.org/10.1016/j.memsci.2007.11.047.

Lin, Y.-S., Chang, C.-H. and Gopalan, R., 1994. "Improvement of Thermal Stability of Porous Nanostructured Ceramic Membranes." *Industrial & Engineering Chemistry Research* 33:860-870. 10.1021/ie00028a012.

Livage, J., Henry, M. and Sanchez, C., 1988. "Sol-gel Chemistry of Transition Metal Oxides." *Prog. Solid St. Chem.* 18:259-341.

Lu, Y., Chen, T., Chen, X., Qiu, M. and Fan, Y., 2016. "Fabrication of TiO2-doped ZrO2 nanofiltration membranes by using a modified colloidal sol-gel process and its application in simulative radioactive effluent." *Journal of Membrane Science* 514:476-486. http://dx.doi.org/10.1016/j.memsci.2016.04.074.

Pierre, A. C., 1998. *Introduction to Sol-Gel Processing*. Springer US

Puhlfürß, P., Voigt, A., Weber, R. and Morbé, M., 2000. "Microporous TiO2 membranes with a cut off <500 Da." *Journal of Membrane Science* 174:123-133. https://doi.org/10.1016/S0376-7388(00)00380-X.

Puthai, W., Kanezashi, M., Nagasawa, H. and Tsuru, T., 2016. "Nanofiltration performance of SiO2-ZrO2 membranes in aqueous solutions at high temperatures." *Separation and Purification Technology* 168:238-247. http://dx.doi.org/10.1016/j.seppur.2016.05.028.

Schaep, J., Vandecasteele, C., Peeters, B., Luyten, J., Dotremont, C. and Roels, D., 1999. "Characteristics and retention properties of a mesoporous γ-Al2O3 membrane for nanofiltration." *Journal of Membrane Science* 163:229-237. https://doi.org/10.1016/S0376-7388(99)00163-5.

Sekulić, J., Magraso, A., ten Elshof, J. E. and Blank, D. H. A., 2004. "Influence of ZrO2 addition on microstructure and liquid permeability of mesoporous TiO2

membranes." *Microporous and Mesoporous Materials* 72:49-57. https://doi.org/10.1016/j.micromeso.2004.04.017.

Shareefdeen, Z., Elkamel, A. and Kandhro, S., 2015. Modern Water Reuse Technologies: Membrane Bioreactors. In S. Eslamian (Eds.) *Urban Water Reuse Handbook* 383-392. doi:10.1201/b19646-41.

Topuz, B., 2009. "Gas permeation through sol-gel derived alumina and silica based membrane." Doctoral thesis, Chemical Engineering, İzmir Institute of Technology.

Topuz, B. and Çiftçioğlu, M., 2010. "Sol–gel derived mesoporous and microporous alumina membranes." *Journal of Sol-Gel Science and Technology* 56:287-299. 10.1007/s10971-010-2305-7.

Tsuru, T., 2008. "Nano/subnano-tuning of porous ceramic membranes for molecular separation." *Journal of Sol-Gel Science and Technology* 46:349-361. 10.1007/s10971-008-1712-5.

Tsuru, T., Narita, M., Shinagawa, R. and Yoshioka, T., 2008. "Nanoporous titania membranes for permeation and filtration of organic solutions." *Desalination* 233:1-9. 10.1016/j.desal.2007.09.021.

Van Gestel, T., Kruidhof, H., Blank, D. H. A. and Bouwmeester, H. J. M., 2006. "ZrO2 and TiO2 membranes for nanofiltration and pervaporation: Part 1. Preparation and characterization of a corrosion-resistant ZrO2 nanofiltration membrane with a MWCO < 300." *Journal of Membrane Science* 284:128-136. http://dx.doi.org/10.1016/j.memsci.2006.07.020.

Van Gestel, T., Vandecasteele, C., Buekenhoudt, A., Dotremont, C., Luyten, J., Leysen, R., Van der Bruggen, B. and Maes, G., 2002. "Alumina and titania multilayer membranes for nanofiltration: preparation, characterization and chemical stability." *Journal of Membrane Science* 207:73-89. http://dx.doi.org/10.1016/S0376-7388(02)00053-4.

Van Gestel, T., Vandecasteele, C., Buekenhoudt, A., Dotremont, C., Luyten, J., Van der Bruggen, B. and Maes, G., 2003. "Corrosion properties of alumina and titania NF membranes." *Journal of Membrane Science* 214:21-29. http://dx.doi.org/10.1016/S0376-7388(02)00517-3.

Voigt, I., Fischer, G., Puhlfürß, P., Schleifenheimer, M. and Stahn, M., 2003. "TiO2-NF-membranes on capillary supports." *Separation and Purification Technology* 32:87-91. http://dx.doi.org/10.1016/S1383-5866(03)00064-9.

Yurtsever, H. A. and Çiftçioğlu, M., 2017. "The effect of rare earth element doping on the microstructural evolution of sol-gel titania powders." *Journal of Alloys and Compounds* 695:1336-1353. http://dx.doi.org/10.1016/j.jallcom.2016.10.275.

Zeidler, S., Puhlfuerss, P., Kaetzel, U. and Voigt, I., 2014. "Preparation and characterization of new low MWCO ceramic nanofiltration membranes for

organic solvents." *Journal of Membrane Science* 470:421-430. 10.1016/j.memsci.2014.07.051.

Zhu, G. Z., Jiang, Q., Qi, H. and Xu, N. P., 2015. "Effect of sol size on nanofiltration performance of a sol-gel derived microporous zirconia membrane." *Chinese Journal of Chemical Engineering* 23:31-41. 10.1016/j.cjche.2014.09.045.

Zhu, J., Fan, Y. and Xu, N., 2011. "Modified dip-coating method for preparation of pinhole-free ceramic membranes." *Journal of Membrane Science* 367:14-20. https://doi.org/10.1016/j.memsci.2010.10.024.